Photocrosslinked Bioreducible Polymeric Nanoparticles for Enhanced Systemic siRNA Delivery as Cancer Therapy

Johan Karlsson,* Stephany Y. Tzeng, Shayan Hemmati, Kathryn M. Luly, Olivia Choi, Yuan Rui, David R. Wilson, Kristen L. Kozielski, Alfredo Quiñones-Hinojosa, and Jordan J. Green*

Clinical translation of polymer-based nanocarriers for systemic delivery of RNA has been limited due to poor colloidal stability in the blood stream and intracellular delivery of the RNA to the cytosol. To address these limitations, this study reports a new strategy incorporating photocrosslinking of bioreducible nanoparticles for improved stability extracellularly and rapid release of RNA intracellularly. In this design, the polymeric nanocarriers contain ester bonds for hydrolytic degradation and disulfide bonds for environmentally triggered small interfering RNA (siRNA) release in the cytosol. These photocrosslinked bioreducible nanoparticles (XbNPs) have a shielded surface charge, reduced adsorption of serum proteins, and enable superior siRNA-mediated knockdown in both glioma and melanoma cells in high-serum conditions compared to non-crosslinked formulations. Mechanistically, XbNPs promote cellular uptake and the presence of secondary and tertiary amines enables efficient endosomal escape. Following systemic administration, XbNPs facilitate targeting of cancer cells and tissue-mediated siRNA delivery beyond the liver, unlike conventional nanoparticle-based delivery. These attributes of XbNPs facilitate robust siRNA-mediated knockdown in vivo in melanoma tumors colonized in the lungs following systemic administration. Thus, biodegradable polymeric nanoparticles, via photocrosslinking, demonstrate extended colloidal stability and efficient delivery of RNA therapeutics under physiological conditions, and thereby potentially advance systemic delivery technologies for nucleic acid-based therapeutics.

1. Introduction

Delivery of exogenous nucleic acids to precisely modulate gene expression in specific cells is recognized to have tremendous potential in the treatment of a wide-range of human diseases.[1] One such technology is RNA interference (RNAi) using small interfering RNA (siRNA) with the ability to cause sequence-specific gene silencing of almost any sequence in the genome upon introduction into a cell. Despite this potential, clinical applications of this technology have been limited due to inefficient siRNA delivery across biological barriers.[2] Delivery technologies using chemically modified siRNA molecules and viral vectors have yet to overcome several limitations, including immunogenicity, limited payload capacity, difficulty of scaled-up vector production, and inefficient silencing.[3,4] In contrast, non-viral nanoparticle-based siRNA delivery formulations have the potential to resolve these major issues as they are generally less immunogenic and easier to manufacture, and enable greater siRNA loading.[5,6]

Dr. J. Karlsson, Dr. S. Y. Tzeng, S. Hemmati, K. M. Luly, O. Choi,
Y. Rui, Dr. D. R. Wilson, Dr. K. L. Kozielski, Prof. J. J. Green
Department of Biomedical Engineering and Institute
for Nanobiotechnology
Johns Hopkins University School of Medicine
Baltimore, MD 21231, USA
E-mail: jkarlss1@jhu.edu; green@jhu.edu
Dr. J. Karlsson
Department of Chemistry–Ångström Laboratory
Uppsala University
Uppsala SE-75121, Sweden

The ORCID identification number(s) for the author(s) of this article can be found under https://doi.org/10.1002/adfm.202009768.

Dr. K. L. Kozielski
Institute for Functional Interfaces
Karlsruhe Institute of Technology
Eggenstein-Leopoldshafen 76344, Germany
Prof. A. Quiñones-Hinojosa
Department of Neurosurgery
Mayo Clinic Florida
Jacksonville, FL 32224, USA
Prof. J. J. Green
Departments of Materials Science and Engineering, Neurosurgery,
Oncology, Ophthalmology, and
Chemical and Biomolecular Engineering
Sidney Kimmel Comprehensive Cancer Center
The Bloomberg~Kimmel Institute for Cancer Immunotherapy
Johns Hopkins University School of Medicine
Baltimore, MD 21231, USA

Recently, the first RNAi technology received regulatory approval using a lipid nanoparticle-based formulation for siRNA delivery for the treatment of polyneuropathies induced by hereditary transthyretin amyloidosis.[7,8] This landmark approval will undoubtedly pave the way for future RNAi nanomedicines and has introduced a new paradigm for genetic medicine.

Nanocarriers for cytosolic delivery of siRNA therapeutics must overcome several challenges for successful knockdown, including efficient cargo encapsulation, cellular uptake by targeted cells, endosomal escape, and timely cytosolic release. In addition, the bioavailability of many nanoparticle systems is often limited to the liver following systemic administration; thus, there is a need for nanomaterials that can enable tissue-mediated extrahepatic delivery as well as for nanomaterials that are biodegradable and nontoxic.[9]

Cationic polymers have shown promise as vectors for nucleic acid delivery given their ability to spontaneously self-assemble with anionic siRNA into condensed nanoparticles with efficient payload encapsulation. Poly(β-amino ester)s (PBAEs) are one class of biodegradable cationic polymers being explored for nucleic acid delivery including for plasmid DNA, and with polymer structural modifications for siRNA.[10–13] This is due to multiple characteristics including their reversible charge, which promotes binding of RNA therapeutics as well as high buffering capacity for endosomal escape, and their degradability by hydrolysis into nontoxic byproducts under aqueous conditions.[14,15] Despite the promising characteristics of PBAEs and cationic nanoparticles in general, positive surface charge when injected often leads to low transfection efficacy following systemic administration due to nonspecific interactions with serum proteins and nanoparticle aggregation, resulting in poor colloidal stability and clearance by the mononuclear phagocyte system.[16,17] To reduce nonspecific protein interactions, one promising strategy is charge-shielding of the nanoparticle surface via either coatings[18] or decationization.[19] In addition, lower surface charge generally decreases the risk of toxicity.[20] The most explored surface modification for charge shielding of nanoparticles is the introduction of poly(ethylene glycol) (PEG) groups via adsorption or conjugation; however, while improving colloidal stability, PEGylation may also impede cellular uptake and endosomal escape, thus decreasing the overall efficacy of the formulation.[21] In addition to charge-shielding, crosslinking is another strategy to improve colloidal stability through covalent stabilization of nanostructures, which otherwise rely on electrostatic interactions, to form robust functional nanomaterials.[22] Photopolymerization for crosslinking to form macroscopic biomaterials has already been proven to allow ease of tuning material properties and scalable fabrication.[23,24] Thus, photocrosslinking is a promising strategy for improving the functionality of nanoscale biomaterials as delivery vehicles.

In this study, we report the engineering of photocrosslinked bioreducible nanoparticles (XbNPs) based on PBAE for nucleic acid-based therapeutics. Addition of a photocrosslinking polymer to PBAE structures yielded fully bioreducible particles with neutral surface charge, decreased nonspecific protein binding, and improved colloidal stability. Although UV-initiated polymerization has previously been demonstrated as a strategy to incorporate acrylate-containing molecules with added functionality for nanoscale delivery systems,[25–28] this is, to our knowledge, the first reported photocrosslinked polymeric nanoparticle platform using a PBAE carrier. Importantly, PBAE-based bioreducible nanoparticles show promise as RNA delivery vectors from a safety perspective, as their bioreducible structure enables environmentally triggered degradation in the reducing environment of the cytosol.[29] Herein, we show that this XbNP platform has the potential to address a variety of challenges facing nanoparticle gene delivery, as the XbNPs demonstrate improved stability in serum, improved cellular uptake, and tissue-mediated delivery to extrahepatic tissues compared to their non-crosslinked counterparts. We used XbNPs to knock down a reporter gene in various patient-derived cancer cell lines and in murine glioblastoma and melanoma cell lines, as well as in a metastatic melanoma model following systemic administration in vivo.

2. Results and Discussion

2.1. Synthesis, Design, and Nanoparticle Characteristics

2.1.1. Synthesis of Bioreducible Polymers and Photocrosslinking of Polymeric Nanoparticles

We used self-assembly to form well-defined nanoparticles.[30,31] The amine-terminated cationic polymer PBAE electrostatically binds anionic siRNA and spontaneously forms nanoscale particles under mildly acidic aqueous conditions (pH = 5.0). In addition to a cationic polymer for siRNA binding, we also added an acrylate-terminated PBAE as the crosslinking polymer (**Figure 1**a). After self-assembly into nanoparticles, we added a radical photoinitiator (Irgacure 2959; Irg) and applied UV light to form crosslinks between the acrylate groups. Both the amine-terminated polymer and the acrylate-terminated polymer for crosslinking contain disulfide bonds in their backbone structures to enable cytosolic glutathione (GSH)-triggered siRNA release. We synthesized the acrylate-terminated crosslinking polymer R64-Ac and the cationic endcap polymers R646/R647 using one- or two-step Michael addition reactions, respectively (Figure 1b). We used gel permeation chromatography (GPC) to measure the polymer molecular weights and to verify crosslinking (Figure 1c). The molecular weight after nanoparticle crosslinking was 42.1% and 27.7% (by M_n and M_w, respectively) greater than that of the non-crosslinked formulation. This increase in molecular weight corresponds to formation of covalent bonds between the acrylate-terminated crosslinking polymers (R64-Ac); and the observed increase is expected, given that the these R64-Ac crosslinking polymers make up 25% of the initial polymer population. In the absence of the photoinitiator, there is no difference in polymer molecular weight with or without UV exposure, indicating a lack of crosslink formation. The short UV exposure time of 1 min is sufficient to form crosslinks and does not cause any measurable degradation of the polymeric nanocarrier. This is a major advantage when using photocrosslinking compared to other crosslinking strategies, since it proceeds quickly under mild reaction conditions.

We also carried out ^{1}H NMR to assess the degree to which acrylate groups were crosslinked. The acrylate peaks were integrated and normalized to peaks corresponding to protons
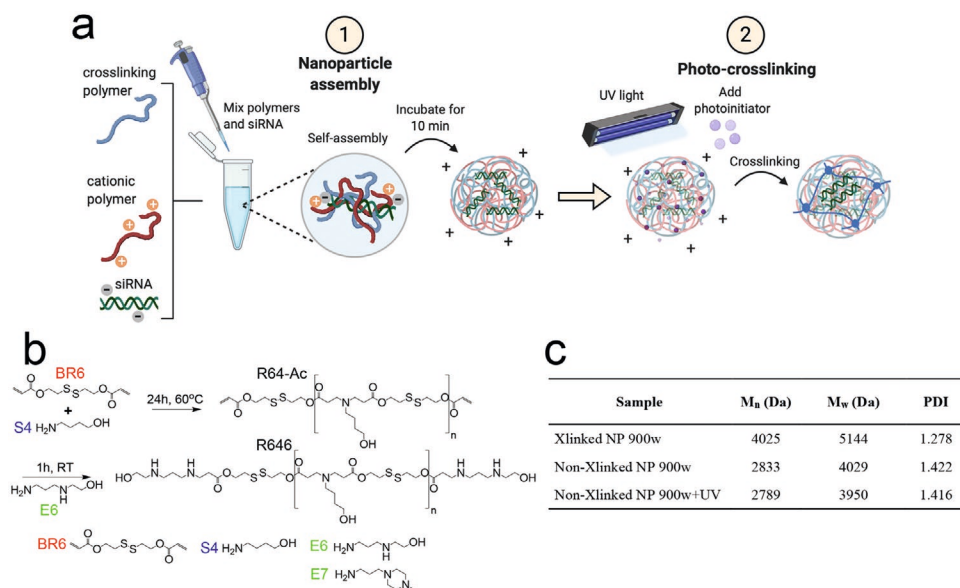
Figure 1. XbNPs for siRNA delivery. a) Schematic illustration of the electrostatic-based self-assembly into nanoparticles (NPs) and subsequent photo-crosslinking. b) Reaction scheme of Michael addition used to form the bioreducible polymers. In the initial step, the diacrylate backbone monomer BR6 is polymerized with the side chain monomer S4 forming the acrylate terminated crosslinking polymer R64-Ac. To form the amine-terminated polymer, a second synthesis step was used, in which the base polymer R64-Ac was endcapped by either monomer E6 or E7 to form R646 and R647, respectively. c) Molecular weight of polymeric nanocarrier assessed by GPC for crosslinked (Xlinked) and non-crosslinked (non-Xlinked) NPs with and without exposure to UV light. The NP formulations were formed at a polymer/siRNA ratio of 900 w/w.

in the backbone of the polymer structure for both crosslinked and non-crosslinked nanoparticle formulations (Figure S1, Supporting Information). The peak intensity of the acrylate peaks decreased 79.1% ± 0.3%, indicating that most of the acrylate groups formed crosslinks. It is possible that not all acrylate groups formed crosslinks due to a lack of other acrylate groups in close proximity with which to react; however, the radical photocrosslinking efficiency seen in the XbNP system is comparable to that seen in similar photopolymerization reactions by other groups.[27] Due to the efficient crosslinking reaction of acrylate groups, the density of covalent crosslinks in the particle can easily be adjusted by altering the ratio between the crosslinking and the amine-terminated polymer. Moreover, to reduce the risk that the added covalent crosslinked network would impede timely intracellular release, we incorporated disulfide bonds into the backbone of both the acrylate- and amine-terminated polymers to facilitate triggered cytosolic release. Cargo release can easily be modulated through incorporation of bioreducible groups and by using PBAE structures with altered hydrophilicity to tune the rate of hydrolytic degradation. The ease of PBAE synthesis is also beneficial for forming polymer structures with diverse chemical properties, which has allowed high-throughput testing of combinatorial libraries of polymers to identify PBAEs structures for efficient transfection of various cell types.[32,33] Further, modulations of the PBAE nanocarriers can also be made for cell-type specificity of nucleic acid therapeutics.[34] These nanoparticle designs have demonstrated the ability to efficiently deliver genes in vivo after local administration.[35,36] However, these previous formulations have had limited success for systemic administration mainly due to insufficient stability in the presence of anionic serum proteins that readily dissociate the formulation

prior to reaching the targeted site.[37] Thus, our XbNP platform could potentially improve extracellular colloidal stability by the addition of covalent bonds, thus improving their likelihood of therapeutic success when administrated systemically. This crosslinked design can also be applied to other cationic polymeric nanoparticles that are formed by self-assembly principles to improve their functionality and stability under physiological conditions to facilitate systemic delivery of nucleic acid therapeutics.

2.1.2. Physical Nanoparticle Properties: Photocrosslinking for Shielded Surface Charge and Reduced Protein Adsorption

We used dynamic light scattering (DLS), nanoparticle tracking analysis (NTA), and transmission electron microscopy (TEM) to assess nanoparticle size and surface charge. We observed no differences in nanoparticle size between crosslinked and non-crosslinked particles; their size was 204 ± 11 nm and 207 ± 12 nm, respectively, measured by DLS at the 60×10^{-9} M siRNA dose and 900 weight ratio polymer to siRNA (w/w) in PBS (**Figure 2**a). Nor did incubation in 10–50% serum influence the size when compared to incubation in PBS (0% serum). In all conditions and by all analytical techniques used, the nanoparticle size was similar both with and without crosslinking (Figure 2a–c). The nanoparticle size decreased slightly with lower siRNA dose and w/w ratios of polymer/siRNA (Figure S2a, Supporting Information; Figure 2f). Further, both the crosslinked and non-crosslinked nanoparticle formulations demonstrated stability in the presence of serum (10% and 50%) until the endpoint of 4 h (Figure 2d,e). It is promising that the nanoparticles remain ≈200 nm in size over time in the
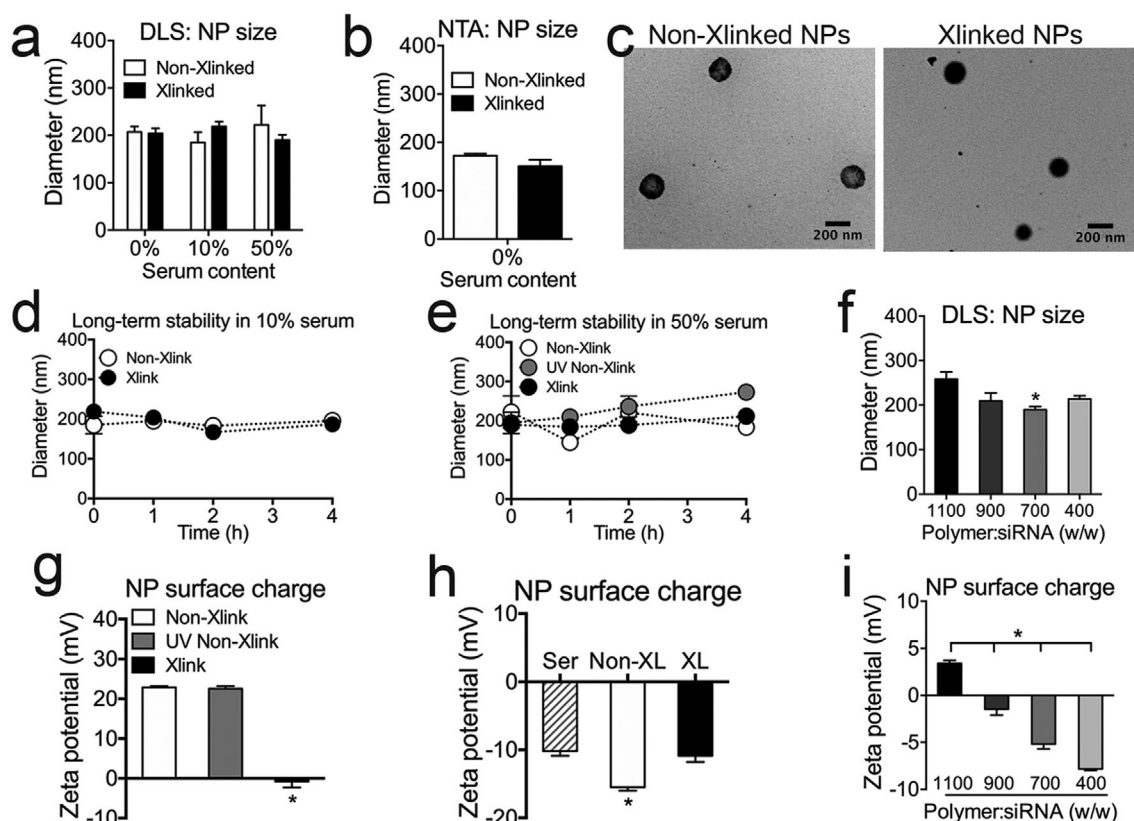
Figure 2. Photocrosslinking reduced the nanoparticle (NP) surface charge of the otherwise cationic nanocarrier. a) NP hydrodynamic diameter assessment by DLS for with (Xlinked) and without (non-Xlinked) crosslinking when incubated in PBS containing 0%, 10%, and 50% serum. b) NTA of NP hydrodynamic diameter. c) Representative TEM images of non-Xlinked (left) and Xlinked (right) NPs. Long-term NP stability assessed with DLS when incubated in d) 10% and e) 50% serum over 4 h. f) The hydrodynamic diameter of NP formulations using different polymer/siRNA ratios (w/w). g) Zeta potential measurements demonstrated reduced surface charge of NPs after crosslinking (*$p < 0.0001$; $n = 3$). h) Surface charge of NPs with (XL) and without (non-XL) crosslinking incubated in 50% serum. The zeta potential for non-XL NPs was statistically lower compared to 50% serum by itself (*$p = 0.0039$; $n = 3$). i) Surface charge of XbNPs formulations using different polymer/siRNA ratios (w/w). One-way ANOVA followed by Tukey's post hoc test was used for statistical analyses. Error bar represents SEM.

presence of serum, as particles between 70 and 200 nm exhibit prolonged circulation.[38]

While nanoparticle sizes were no different between the crosslinked and the non-crosslinked formulations, zeta potential measurements demonstrated that crosslinking reduced the surface charge from +22.9 ± 0.3 mV for the non-crosslinked nanoparticles to being neutral (–0.8 ± 1.5 mV) after crosslinking (Figure 2g). This shielding of the cationic charge is beneficial for promoting colloidal nanoparticle stability in the bloodstream, as interactions with anionic serum proteins may lead to nanoparticle dissociation and loss of encapsulated siRNA during circulation.[1,16] Poor colloidal stability may influence experimental outcomes, both in vitro and in vivo, by affecting mechanisms such as cellular uptake and increasing overall toxicity,[39] and is a leading reason why cationic nanoparticles have not been sufficiently effective at the delivery of RNA therapeutics upon systemic administration.[40] Moreover, nanoparticle formulations should avoid adsorption of serum opsonins to prevent recognition and clearance by the mononuclear phagocyte system.[17] Thus, nanoparticles that interact less with the biological environment are desirable for prolonged circulation to reach targeted tissues. Some cationic nanocarriers require

surface modifications to minimize nonspecific interactions, with the most common approach being PEGylation of the nanoparticle surface for steric shielding.[41] However, the incorporation of PEG may reduce the degree of intracellular delivery of RNA therapeutics, thus these systems may require PEG de-shielding for successful intracellular trafficking.[21,41,42] Decationization is another strategy to improve the circulation time when using cationic polymeric nanocarriers, in which the polymer undergoes hydrolysis of cationic groups to form neutral or negatively charged nanoparticles prior to administration.[19] In this study, we have demonstrated that photocrosslinking can shield the surface charge that is otherwise positive due to the cationic polymer, eliminating the need for additional modifications to achieve neutral surface charge. Further, the crosslinked nanoparticles can be tuned to be slightly positive or negative by adjusting the ratio between the cationic polymer and the RNA dose (Figure 2i). UV exposure times as short as 0.5 min are sufficient for loss of the cationic charge (Figure S2f, Supporting Information).

When incubated in serum, the non-crosslinked nanoparticles demonstrated statistically lower surface charge ($p = 0.0039$; $n = 3$) than the serum itself, whereas no difference
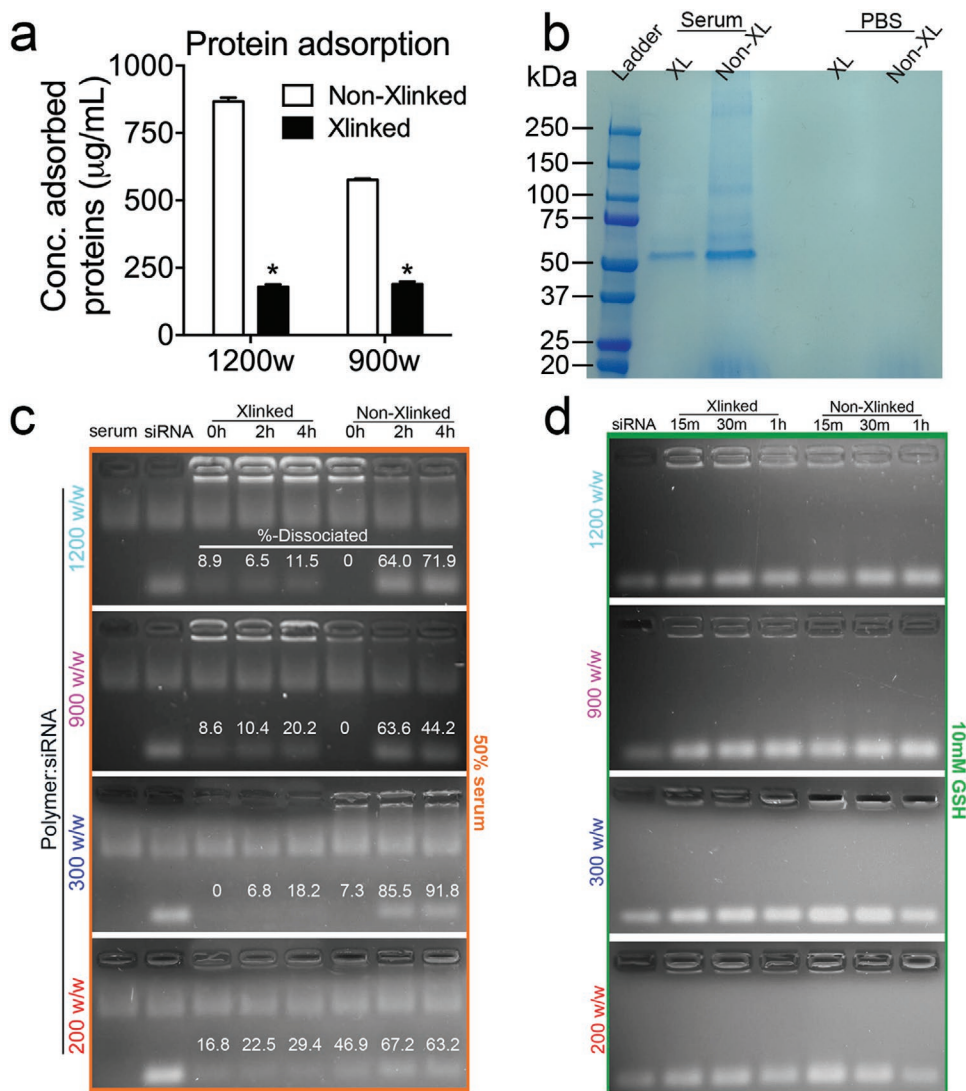
**ADVANCED
SCIENCE NEWS**

www.advancedsciencenews.com

**ADVANCED
FUNCTIONAL
MATERIALS**

www.afm-journal.de

Figure 3. XbNPs lowered protein adsorption when incubated in serum and improved siRNA encapsulation efficiency in a high-serum condition. a) The protein adsorption was assessed by the BCA assay for crosslinked (Xlinked) and non-crosslinked (non-Xlinked) NPs using formulations of 1200 and 900 w/w ratios ($n = 3$). *$p < 0.0001$, as determined by two-way ANOVA followed by Sidak's multiple comparison. Error bars represent SEM. b) SDS–PAGE of adsorbed proteins following incubation in serum or PBS for nanoparticles with (XL) and without (non-XL) crosslinking. Gel electrophoresis assessment of c) siRNA-encapsulation efficiency for crosslinked (Xlinked) and non-crosslinked (non-Xlinked) NPs using formulations of 1200, 900, 300, and 200 w/w ratios when incubated in 50% serum for 4 h, and d) siRNA release when incubated in cytosolic-mimicking environment of 10×10^{-3} M GSH.

was observed for the XbNPs (Figure 2h). This indicates that there is higher adsorption of serum proteins to the non-crosslinked nanoparticles, thus conferring anionic charge. We first assessed the ability of photocrosslinking to alter protein adsorption under high serum conditions using a bicinchoninic acid (BCA) assay. We compared the amount of protein adsorbed onto both non-crosslinked and crosslinked nanoparticles across two different weight ratios, 1200 and 900 w/w. The protein adsorption was significantly lower for the XbNPs for both the 1200 and 900 w/w formulations (**Figure 3**a). This is likely due to the decrease in nanoparticle surface charge following photocrosslinking, thus reducing the ionic interactions between the nanoparticles and anionic serum proteins (Figure 2g). The decreased interactions with serum proteins may aid in XbNPs'

translation as a delivery technology for systemic administration, as the otherwise major limiting hurdle when using cationic polymeric nanocarriers is the competitive binding of polyanions that destabilize the formulation.[37]

While protein adsorption following intravenous (i.v.) injection results in a protein corona around the nanoparticle, which might impede intracellular delivery, adsorption of specific serum proteins may be beneficial for mediating cell- and tissue-specific delivery.[16,43–46] We therefore further examined the composition of the adsorbed proteins by running sodium dodecyl sulfate–polyacrylamide gel electrophoresis (SDS–PAGE) on crosslinked and non-crosslinked nanoparticles after incubation in serum and in PBS as control. In the serum condition, the XbNPs displayed fewer bands of lower intensity

(Figure 3b), which supports the finding from the BCA assay that photocrosslinking lowers the overall protein adsorption. The most distinct band of the adsorbed proteins onto both the crosslinked and non-crosslinked nanoparticles was at 58 kDa, corresponding to albumin, which is one of the most abundant proteins found in serum and has been shown to promote receptor-mediated nanoparticle uptake in cancer cells.[47] This phenomenon is due to increased albumin metabolization by cancer cells to support energy and amino acid consumption associated with rapid cancer-cell proliferation.[27,28] It is therefore possible that adsorption of high-molecular-weight proteins shields adsorbed albumin, leading to decreased cellular uptake of the non-crosslinked nanoparticle formulations. The results from the SDS–PAGE assay indicate that non-crosslinked nanoparticles adsorb greater amounts of proteins with a molecular weight above 58 kDa than their XbNP counterpart, suggesting that the crosslinked nanoparticles might promote cellular uptake. The specific interaction with albumin for the XbNPs is interesting since it potentially could be useful for biomimetic targeting and tumor accumulation.[48]

2.1.3. Photocrosslinking Promotes Colloidal Nanoparticle Stability

We performed siRNA gel electrophoresis assay to evaluate the colloidal nanoparticle stability and the encapsulation efficiency over time. We prepared crosslinked and non-crosslinked nanoparticle formulations with weight ratios (w/w) 1200, 900, 300, and 200 and incubated them in 50% serum over 4 h. The dissociation of the nanoparticles, measured by release of the siRNA payload, was markedly lower for the crosslinked particles across all tested formulations both after 2 and 4 h, with the majority of the siRNA dose dissociated from the non-crosslinked formulations at 2 h (Figure 3c). Thus, photocrosslinking of the nanoparticle formulations improves the encapsulation efficiency and colloidal stability of the particles under high-serum conditions. The reduced surface charge and corresponding decreased interactions with serum proteins are advantageous as cationic polymeric carriers rely on electrostatic interactions to bind and encapsulated RNA molecules. These cationic polymer/siRNA nanocomplexes can easily dissociate due to competitive binding of cationic polymer to other anionic biomolecules.[37] Competitive binding to anionic proteins in serum is a likely cause of the observed higher degree of nanoparticle dissociation and siRNA release for the non-crosslinked formulations. We also carried out a gel electrophoresis assay after nanoparticle incubation in a cytosolic-mimicking environment (10×10^{-3} M GSH)[49,50] to examine whether the crosslinking would affect the intracellular release kinetics. The high concentration of GSH in the cytosol readily cleaves disulfide bonds upon entry to the cytosol, leading to release of encapsulated molecules.[23,24,47] Across the tested formulations using 1200, 900, 300, and 200 w/w, we observed no delay in the siRNA release in the cytosolic-mimicking environment for the crosslinked nanoparticles compared to the non-crosslinked nanoparticles (Figure 3d). Both the crosslinked and non-crosslinked particles exhibited triggered siRNA release in the reducing environment within 15 min. This is due to the presence of disulfide bonds in the structure of both of the polymers used for nanoparticle formation. The similar release kinetics between non-crosslinked and crosslinked nanoparticles indicate that crosslinking does not interfere with rapid intracellular release of RNA therapeutics delivered by these bioreducible polymeric carriers. The incorporation of stimuli-responsive crosslinks in the nanoparticle formulations that rely on electrostatic interactions for improved colloidal stability in the blood stream and in extracellular spaces holds great promise for successful translation.[20,51] A strategy of high interest is the use of environmentally triggered crosslinks containing disulfide bonds, since these materials provide stability during extracellular circulation while being readily cleaved in cytosol due to the high concentration of GSH leading to a quick release of the payload.[50,52,53] In our XbNP design, both the acrylate-terminated and the amine-terminated polymers contained disulfide bonds for triggered cytosolic release while preventing nanoparticle dissociation prior to being internalized into targeted cells.

2.2. In Vitro siRNA Delivery: Photocrosslinked Nanoparticles as a Platform for Intracellular Delivery to Cancer Cells

2.2.1. Crosslinked Nanoparticles Mediate siRNA Delivery in Patient-Derived Cancer Cells under High-Serum Conditions

We evaluated the siRNA delivery efficacy of the engineered XbNP formulations under high-serum conditions (50% serum) to better mimic the environment of the bloodstream after systemic delivery, with patient-derived glioblastoma cells (GBM319) as the first cancer cells tested. To modulate the degree of crosslinking, we varied the ratio between the acrylate polymer (R64Ac) and end-capped polymer (R646), and nanoparticles were formulated with and without photocrosslinking. For all the ratios tested, the crosslinked formulations provided superior siRNA-mediated GFP knockdown in the GBM319 human brain cancer cells compared to the matched non-crosslinked formulations with an optimized mass ratio of 1:3 (R64Ac to R646) causing 83% ± 5% silencing of GFP expression (**Figure 4**a). We then explored the duration of UV exposure needed for photocrosslinking, and we observed that only 0.5 min of UV exposure was required to achieve efficient transfection in high-serum conditions, with no significant difference measured for UV exposures between 0.5 and 2 min (Figure 4b). When UV exposure lasted for 3 min or longer, siRNA-mediated knockdown decreased significantly, likely due to degradation of the polymer.

We also compared nanoparticle formulations with varying weight ratios (w/w) between the polymer and siRNA dose, as were those containing amine-terminated polymers with different endcaps (termed R646 or R647). For all tested formulations, the crosslinked nanoparticles outperformed their non-crosslinked counterparts, and the formulations with R646 led to the greatest transfection of up to 96% ± 2% siRNA-mediated GFP knockdown (Figure 4c,d; Figure S3a, Supporting Information). This great efficacy observed under high-serum conditions shows the tremendous potential of XbNPs to be used as a nanoparticle platform for systemic siRNA delivery. The presence of serum in culture media generally interferes with in vitro transfection. Polyethylenimine (PEI), for instance, is a commonly used nanocarrier with efficient transfection capability in serum-free
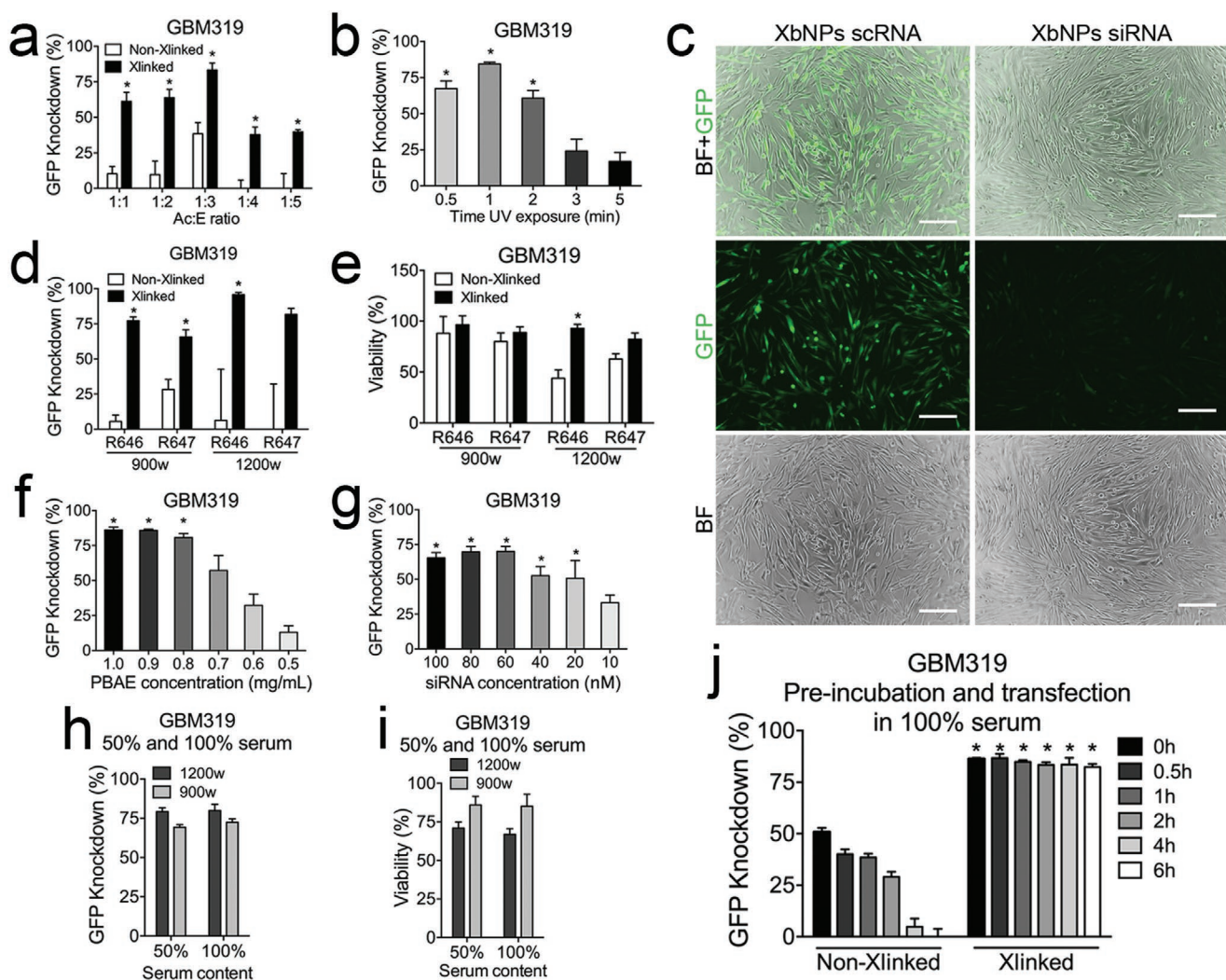
Figure 4. XbNPs provided superior siRNA-mediated knockdown in patient-derived glioblastoma cells (GBM319) in high-serum conditions and following preincubation for 6 h compared to non-crosslinked nanoparticles (NPs). In vitro transfection in 50% serum of GBM319-GFP$^+$ cells assessed by flow cytometry analyzing siRNA-mediated knockdown for a) crosslinked (Xlinked) and non-crosslinked (non-Xlinked) NPs formulated with different ratio of acrylate-terminated (Ac) and amine-endcapped (E) polymers (*$p < 0.0001$; two-way ANOVA followed by Sidak's multiple comparisons) and b) Xlinked NPs prepared with different UV exposure times (*$p < 0.0001$; one-way ANOVA). c) Representative fluorescence microscopy images of GBM319-GFP$^+$ treated with XbNPs carrying either scRNA or siRNA targeting GFP (scale bars = 200 μm). d) siRNA-mediated knockdown (*$p < 0.05$; two-way ANOVA followed by Sidak's multiple comparisons) and e) viability (*$p < 0.005$; two-way ANOVA followed by Sidak's multiple comparisons) assessed by MTS assay for transfection in 50% serum of non-Xlinked and Xlinked NPs formulated with either R646 or R647 as the amine-terminated polymer using 900 or 1200 w/w formulations. siRNA-mediated knockdown of XbNPs with altered f) polymer (*$p < 0.0001$; one-way ANOVA followed by Tukey's post hoc test) and g) siRNA (*$p < 0.01$; one-way ANOVA followed by Tukey's post hoc test) concentrations. h) siRNA-mediated knockdown and i) viability in GBM319 when transfected with XbNPs in 50% and 100% serum. j) Transfection following preincubation at varied times in complete serum (*$p < 0.0001$; two-way ANOVA followed by Sidak's multiple comparisons). Error bars represent SEM and $n = 4$.

media; however, the addition of just 10% serum drastically decreases its efficacy.[54] Not only did photocrosslinking improve the transfection efficacy of the nanoparticles, but it also reduced toxicity. At the highest tested polymer concentration prepared, the 1200 w/w ratio, a 50% decrease in viability was observed for the R646-based non-crosslinked formulation, whereas the photocrosslinked formulation showed minimal toxicity (Figure 4e). The reason for the reduced toxicity is likely due to the shielded surface charge after photocrosslinking, as cationic nanoparticles have been shown to exhibit increased toxicity compared to neutral or anionic particles.[55]

Further, we evaluated the polymer concentrations and siRNA doses required for high transfection efficacy in high-serum conditions. For the polymer, a concentration of 0.8 mg mL^{-1} or higher is required to achieve greater than 75% siRNA-mediated knockdown (Figure 4f). For the siRNA dose, there was no statistical difference in the transfection between the doses of 20×10^{-9} and 100×10^{-9} M, which shows that the photocrosslinked nanocarrier provided highly potent siRNA delivery to patient-derived glioblastoma cells (Figure 4g) at low dose. Low toxicity was observed across all the tested crosslinked nanoparticle formulations (Figure S3b–d, Supporting Information). We observed no
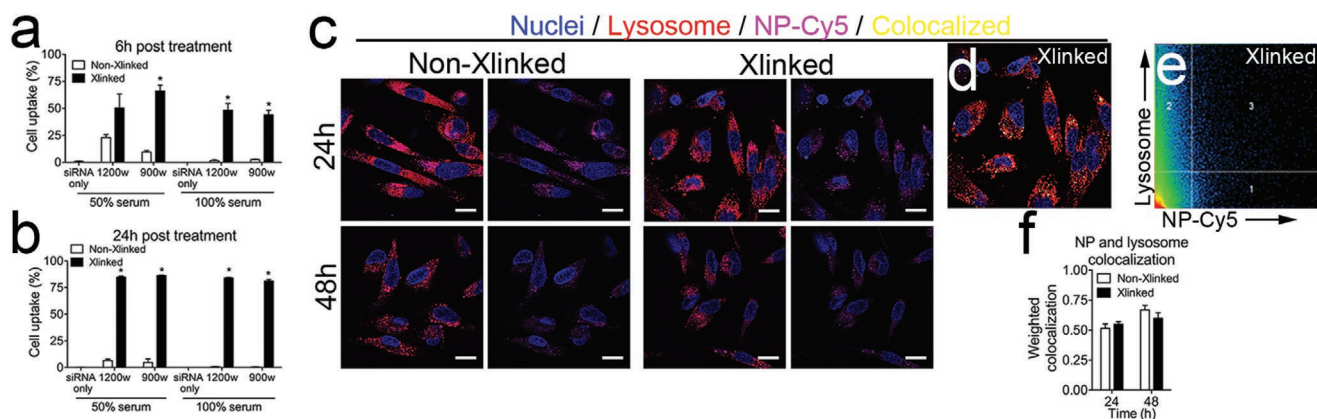
Figure 5. XbNPs enhanced cellular uptake compared to non-Xlinked NPs in patient-derived glioblastoma cells (GBM319) upon transfection in high-serum conditions. Cellular uptake in GBM319 cells assessed by flow cytometry after a) 6 h (*$p < 0.0001$; $n = 4$) and b) 24 h (*$p < 0.0001$; $n = 4$) following transfection in 50% and 100% serum for crosslinked (Xlinked) and non-crosslinked (non-Xlinked) nanoparticles (NPs) carrying Cy5-labeled siRNA. c) Confocal microscopy images of cellular uptake for NP carrying Cy5-labeled siRNA 24 and 48 h posttreatment (scale bars = 20 μm). d) Representative image 24 h posttreatment with XbNPs showing nanoparticle (Cy5) and lysosome/endosome colocalization in yellow. e) Representative 2D scattergram 24 h posttreatment with XbNPs, in which region 3 represents colocalized pixel intensities. f) NP and lysosome/endosome colocalization 24 and 48 h post-treatment with Xlinked and non-Xlinked NPs ($n = 3$). Two-way ANOVA followed by Sidak's multiple comparisons were used for statistical analyses. Error bars represent SEM.

cellular toxicity for the photocrosslinker Irg at the transfection concentration of 0.17 mg mL^{-1} and the concentration can even be increased at least by a magnitude to 1.7 mg mL^{-1} without any toxicity issues (Figure S3e, Supporting Information). Williams et al. demonstrated in their study that Irg (Irgacure 2959) is well tolerated by many cell types and species.[56]

2.2.2. Long-Term Colloidal Nanoparticle Stability Following Preincubation in Serum without Loss in Efficacy

We also evaluated the efficacy of the engineered nanoparticles in complete (100%) serum conditions to model systemic administration. The XbNPs demonstrated the same degree of siRNA-mediated knockdown in patient-derived glioblastoma cells in complete serum as in 50% serum condition with low toxicity (Figure 4h,i). To examine the long-term colloidal nanoparticle stability in complete serum, we pre-incubated the XbNPs and non-crosslinked particles in 100% serum at 37 °C for up to 6 h prior to transfection experiments in complete serum. The degree of siRNA-mediated knockdown decreased as pre-incubation time increased for the non-crosslinked nanoparticles, whereas knockdown with the XbNPs was unaffected: even after 6 h of pre-incubation in complete serum, XbNPs caused 82% ± 2% GFP knockdown (Figure 4j). Together, the long-term stability and high transfection efficacy under high-serum conditions show the promise of the XbNP platform for systemic siRNA delivery.

2.2.3. Cellular Uptake and Endosomal Escape of Engineered Nanoparticle Formulations

To elucidate the mechanisms of the improved siRNA delivery efficacy for the XbNPs, we evaluated cellular uptake and endosomal escape in patient-derived glioblastoma cells at

high-serum conditions. In these experiments, Cy5-siRNA was used, and cellular uptake was initially compared at different time-points post-transfection. After both 6 and 24 h post-treatment and in both 50% and 100% serum, the XbNPs were taken up by cells more efficiently than non-crosslinked nanoparticles (**Figure 5a**,b; Figure S4, Supporting Information). To study endosomal escape, we used confocal microscopy to visualize the nuclei and lysosomes, along with the Cy5-siRNA in the nanoparticle formulations (Figure 5c). We evaluated endosomal escape by quantifying the colocalization of the lysosomes and Cy5-nanoparticles, with lower colocalization corresponding to effective endosomal escape. The results showed no differences between the crosslinked and non-crosslinked nanoparticle formulations, demonstrating that the shielded charge following photocrosslinking does not significantly affect endosomal escape (Figure 5d–f). Thus, the mechanism through which XbNPs facilitate enhanced siRNA-mediated knockdown is thought to be via improved cellular uptake. The XbNPs with improved encapsulation of siRNA, prolonged particle stability in pure serum (Figure 3c), and reduced adsorption of high-molecular-weight proteins (such as immunoglobulins) (Figure 3b) enhance cellular uptake.

2.2.4. Nanoparticle Platform for siRNA Delivery to Various Glioma Cells

We evaluated XbNPs for their potential to serve as a platform for efficient siRNA delivery to other glioblastoma cell lines. This is of importance because brain tumors are heterogeneous;[57] hence, robust delivery to various brain cancer cells is required for effective treatment of glioma patients. We tested the nanoparticle formulations in GBM1A, a patient-derived glioblastoma cell line with high stemness.[58] Stem-like glioma cells are extremely evasive and resistant when it comes to radiation therapies[59] and contribute greatly to disease progression.[60] Novel
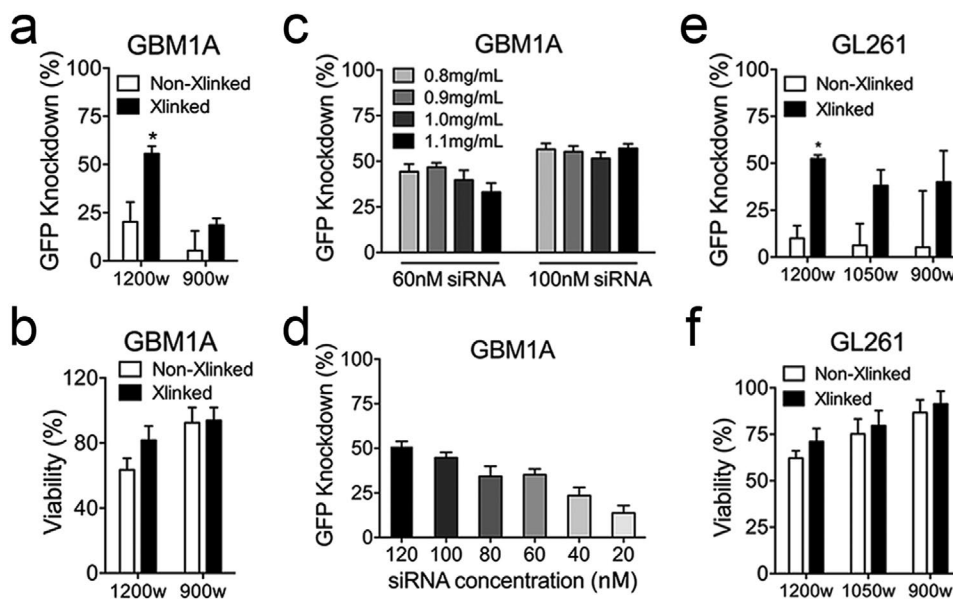
Figure 6. XbNPs provided robust siRNA-mediated knockdown in various glioblastoma cell lines in high serum (50%) conditions. a) siRNA-mediated knockdown (*$p < 0.01$) assessed by flow cytometry and b) viability assessed by the MTS assay in GBM1A cells following treatment of crosslinked (Xlinked) and non-crosslinked (non-Xlinked) nanoparticles using 1200 and 900 w/w formulations. c) Transfection of GBM1A using XbNP formulations with varied polymer concentrations (0.8–1.1 mg mL^{-1}) and siRNA doses (60 and 100×10^{-9} M), corresponding to 500–1200 w/w and d) dose-dependent (10×10^{-9}–120×10^{-9} M) siRNA-mediated knockdown for XbNPs. e) siRNA-mediated knockdown (*$p < 0.05$) and f) viability in GL261 cells following treatment with XbNPs using 1200, 1050, and 900 w/w formulations. Two-way ANOVA followed by Sidak's multiple comparison were used for statistical analyses. Error bars represent SEM and $n = 4$.

therapeutics for glioblastoma must be able to address glioma cells broadly, including those with stem-like properties, in order to control disease progression. In GBM1A, XbNPs at 1200 w/w achieved >50% siRNA-mediated GFP knockdown while still having low toxicity (**Figure 6a**,b). Over a range of siRNA dose from 20×10^{-9} to 120×10^{-9} M and polymer doses from 0.8 to 1.1 mg mL^{-1}, corresponding to 500–1200 w/w, knockdown was observed to be ≈10–50% (Figure 6c,d), with knockdown in GBM1A stem-like brain cancer cells especially sensitive to siRNA dose.

The XbNPs were also evaluated in GL261 cells, a commonly used murine glioma model. As in the GBM1A cells, the XbNP formulation of 1200 w/w caused >50% GFP knockdown with low cytotoxicity (Figure 6e,f). Together, as observed in the patient-derived glioblastoma cell line GBM319, the XbNP formulations also outperformed the non-crosslinked formulations in GBM1A and GL261 cells in terms of siRNA-mediated knockdown. The results suggest that the XbNPs could potentially serve as a next-generation nanoparticle platform for siRNA-based therapeutics for glioma. Their ability to transfect diverse glioma cells is crucial given the intrinsic heterogeneity of glioblastoma,[57] and future genetic therapeutics that address the heterogeneous cell population may lead to improved outcomes for glioma.

2.2.5. Photocrosslinked Nanoparticles for siRNA Delivery to Melanoma Cells

We further evaluated the XbNPs' ability to provide siRNA-mediated knockdown in murine melanoma cells (B16F10) in

high-serum conditions (50% serum). The XbNPs outperformed their non-crosslinked counterparts in terms of both increased knockdown efficacy and reduced toxicity (**Figure 7a**–c).

A critical property of nanocarriers to enable potent systemic delivery of siRNA is high and stable encapsulation of the siRNA therapeutics. To assess the encapsulation efficiency, we performed a RiboGreen RNA assay, in which we increased the siRNA dose while keeping polymer concentration constant to modulate the w/w of nanoparticle formulations. Across all the tested nanoparticle formulations (200–800 w/w), efficient siRNA encapsulation was observed (Figure 7d), with the XbNPs at 270 w/w showing statistically higher siRNA encapsulation than the non-crosslinked formulation. Higher siRNA payload promotes transfection efficacy, as the 400 w/w formulation provided almost complete siRNA-mediated GFP knockdown (Figure 7e).

2.2.6. Gal8-Assay Demonstrates Improved Cellular Uptake in Melanoma Cells for Crosslinked Nanoparticles

Critical hurdles for successful intracellular delivery of nucleic acid-based therapeutics involve cellular uptake and endosomal escape. Nanoparticle endocytosis must be followed by endosomal escape for successful delivery; otherwise, endosomal entrapment renders the nanoparticle and its cargo useless as it is degraded via the endo/lysosomal pathway.[61] For polymeric nanoparticles with titratable amine groups, endosomal escape occurs in part as the internalized particle buffers pH changes in the endocytic vesicle, ultimately leading to an increase in osmotic pressure and subsequent vesicle rupture
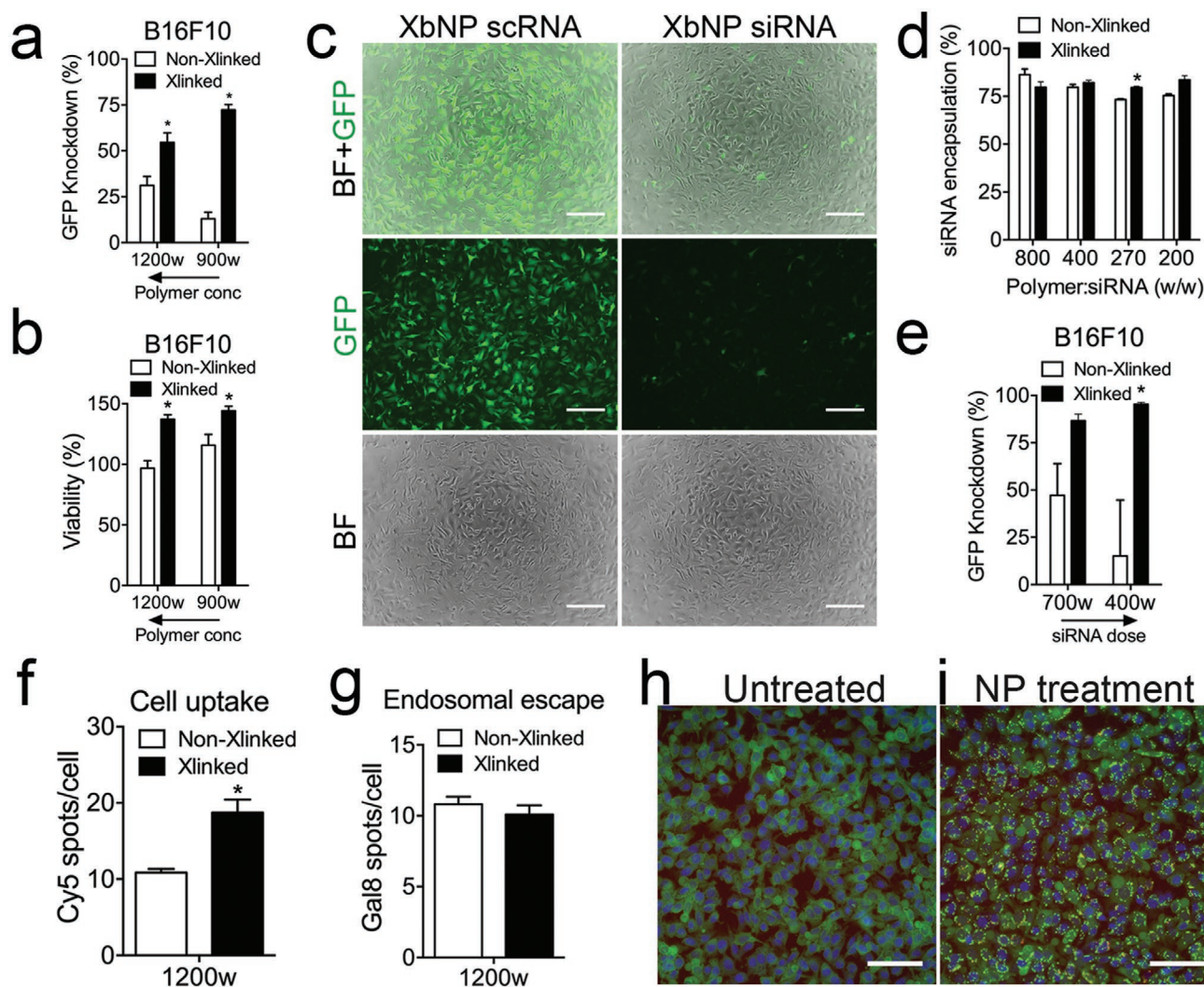
Figure 7. XbNPs facilitated superior siRNA-mediated knockdown in murine melanoma cells (B16F10-GFP[+]) in high serum (50%) conditions compared to non-crosslinked nanoparticles (NPs) attributed by improved cellular uptake. a) GFP knockdown (*$p < 0.0001$; $n = 4$; two-way ANOVA followed by Sidak's multiple comparisons) assessed by flow cytometry and b) viability (*$p < 0.0001$; $n = 4$; two-way ANOVA) assessed by MTS following treatment with crosslinked (Xlinked) and non-crosslinked (non-Xlinked) NPs using 1200 and 900 w/w formulations with altered polymer concentration. c) Representative fluorescence microscopy images of B16F10-GFP[+] treated with XbNPs carrying either scRNA or siRNA targeting GFP (scale bars = 200 µm). d) siRNA encapsulation efficiency for nanoparticles with various w/w formulations assessed by RiboGreen assay (*$p = 0.020$; $n = 2$; Holm–Sidak corrected multiple Student's t-test). e) siRNA-mediated knockdown in B16F10 cells using 700 and 400 w/w NP formulations with altered siRNA dose (*$p < 0.005$; $n = 4$; two-way ANOVA followed by Sidak's multiple comparisons). Assessment of f) cellular uptake quantified by Cy5 spots per cell (*$p < 0.0001$; $n = 3$; two-tailed Student's t-test) and g) endosomal escape quantified by Gal8-GFP^{+} per cells in B16F10 cells using the Gal8-GFP recruitment assay, in which the NPs used contained Cy5-labeled siRNA. Representative images of Gal8-GFP^{+} B16F10 cells h) without treatment and i) after treatment with NPs (scale bars = 100 µm). Error bars represent SEM.

and nanoparticle release.[62] This mechanism, termed the "proton sponge effect," has been the subject of debate among groups studying nanoparticle-based drug and gene delivery.[62] Although elucidation of the exact mechanisms underlying endosomal escape of PBAEs is still under active investigation, a recently developed assay utilizing Gal8 to visualize endosomal disruption allows the quantitative assessment of nanoparticle endosomal escape in vitro.[63] We used this method to evaluate cellular uptake and endosomal disruption in B16F10 cells, in which the XbNP and non-crosslinked formulations contained Cy5-siRNA and the B16F10 cells expressed a Gal8-GFP fusion protein. In the assessment of cellular uptake

quantifying Cy5-spots/cell, statistically higher uptake was demonstrated for the XbNPs compared to non-crosslinked nanoparticles (Figure 7f). To assess endosomal escape, we quantified Gal8-GFP spots/cell, corresponding to the number of endosomal disruption events.[63] Endosomal escape was not different between the XbNPs and non-crosslinked nanoparticles (Figure 7g). Representative microscopy images from the Gal8-assay comparing untreated and nanoparticle-treated cells (Figure 7h,i) clearly demonstrate how efficient the engineered PBAE nanocarrier is at facilitating endosomal disruption for intracellular siRNA delivery to the cytoplasm. This demonstrates that the mechanism for improved siRNA delivery

efficacy of the XbNPs in B16F10 cells is improved cellular uptake of siRNA, which is in line with the mechanistic results found in patient-derived glioblastoma cells. Additionally, the XbNP formulation contains both secondary and tertiary amines that undergo protonation at the lower pH of the endosomal compartment leading to osmotic pressure, which causes endosomal disruption. The results indicate that, despite the surface charge-shielding due to photocrosslinking, amines remain accessible for buffering in the XbNP formulation, thus leaving the desirable endosomal escape efficiency unchanged.

2.3. Photocrosslinked Nanoparticles for Systemic siRNA Delivery to Tumors In Vivo

2.3.1. Tissue-Mediated Nanoparticle Delivery

We evaluated the XbNPs for systemic siRNA delivery following i.v. injection. We initially used XbNPs containing IR-labeled siRNA to evaluate biodistribution after systemic administration. This study demonstrated that photocrosslinking PBAE nanoparticles improved targeting to the lungs (**Figure 8a**,b; Figure S5, Supporting Information). In addition, both XbNPs and non-crosslinked nanoparticles facilitated siRNA delivery to the brain to some degree. This finding is in agreement with a recent study showing that non-crosslinked PBAE nanoparticles facilitated active transport across a biomimetic in vitro assay of the BBB endothelium and delivery to the brain in vivo following systemic administration.[12] This result might be due in part to the adsorption of albumin shown for both XbNPs and non-crosslinked PBAE nanoparticles (Figure 3b). Lin et al. demonstrated that their albumin-based nanoparticles facilitated BBB crossing via mechanisms of SPARC and gp60-mediated transport.[64] Moreover, differences in cumulative fluorescent intensity observed between crosslinked and non-crosslinked formulations are most likely due to the nanoparticles that did not extravasate and accumulate in organs, but instead were excreted in urine and stool.

To broaden the potential of nanomedicine carrying RNA therapeutics, there is a need for nanocarriers capable of extra-hepatic delivery. The recent success of the lipid nanoparticle formulation Onpattro that was FDA-approved in 2018 demonstrated liver-targeted siRNA delivery for the treatment of polyneuropathies.[8] Based on learnings from Onpattro's clinical success, key features required for clinical translation are low surface charge and efficient siRNA encapsulation, both of which are facilitated by photocrosslinking in this study. Despite early translational success for RNA-based therapies, the challenge remains to develop nanoparticle designs for delivery targeted to tissues beyond the liver. The Onpattro lipid nanoparticles facilitate adsorption of apolipoprotein E (ApoE; 34 kDa) following i.v. administration, leading to delivery to hepatocytes.[8] In contrast, our XbNPs have specific affinity to albumin (58 kDa; Figure 3b), which facilitates different biodistribution. A key factor that likely correlates with the protein adsorption is the nanoparticle surface charge, which can dictate tissue-targeting. Cheng et al. developed a lipid nanoparticle system termed selective organ targeting (SORT) in which they modulated the lipid composition of nanoparticles and thereby altered the surface charge through which they were able to achieve tissue-specific mRNA delivery.[65] They demonstrated lung-targeted delivery of their neutrally charged lipid nanoparticle formulation, which is consistent with the current findings. Through slight changes of the surface charge via tuning of the lipid composition, the tissue specificity of the SORT nanoparticles could be tailored. In a non-lipid nanocarrier system, we demonstrate for XbNPs that altered ratios between polymer and siRNA enabled differential tissue targeting. XbNPs using 400 w/w ratio facilitated preferential organ delivery to the spleen (Figure 8c,d). When comparing the radiant efficiency of each organ to all analyzed organs for each formulation, the XbNPs using 900 w/w facilitated statistical higher delivery to the lungs and the XbNPs using 400 w/w facilitated preferential delivery to the spleen (Figure 8e). The differential tissue targeting observed is likely due to difference in surface charge that can be easily tuned by altering the amount of polymer mixed with siRNA during the self-assembly step of the XbNP formulation (Figure 2i).

2.3.2. Preferential Uptake in Cancer Cells and siRNA-Mediated Knockdown In Vivo

Melanoma cells are highly metastatic and commonly metastasize to the lungs.[66] To establish an in vivo model to approximate melanoma metastasis to the lungs, we injected melanoma cells i.v. that expressed luciferase and tdTomato (B16F10-Luc = tdTomato$^+$). IVIS imaging of the bioluminescence showed that the melanoma cells colonized and formed tumors in the lungs and grew exponentially over time (Figure S6, Supporting Information).

We established a similar model by creating B16F10 tumors expressing GFPd2 to analyze nanoparticle uptake in different cell types of the lungs. We administered XbNPs containing Cy5-siRNA i.v. and harvested the lungs after 18 h. We assessed nanoparticle uptake by specific cell populations by flow cytometry, measuring internalization in cancer cells, epithelial cells (CD31$^+$), endothelial cells (CD326$^+$), and hematopoietic cells (CD45$^+$). The nanoparticle uptake by the melanoma cells was statistically higher compared to all other phenotypes (Figure 8f; $p = 0.0033$; $n = 5$), demonstrating that the XbNPs selectively targeted cancer cells over other cell types in the lungs. Preferential delivery to cancer cells has been observed for certain PBAE structures in previous in vitro studies. Sunshine et al. explored DNA delivery using a PBAE nanocarrier in a wide-range of cell types and showed that modulations of the small-molecular endcaps strongly influence cell-specificity.[34] Other studies using PBAEs as vectors for either DNA or siRNA therapeutics have demonstrated preferential delivery to cancer cells over healthy cells as a result of modulation of the polymer structure.[11,67–69] These in vitro transfection studies were all performed in low-serum conditions, allowing the intrinsic properties of PBAEs to facilitate preferential delivery. In the case of XbNPs, the decreased nonspecific interactions with serum proteins after administration into the bloodstream suggest that PBAEs can enable preferential delivery to cancer cells even after i.v. administration. In addition, the specific protein interaction of albumin with the nanoparticle surface after photocrosslinking may serve as another mechanism for tumor targeting, since
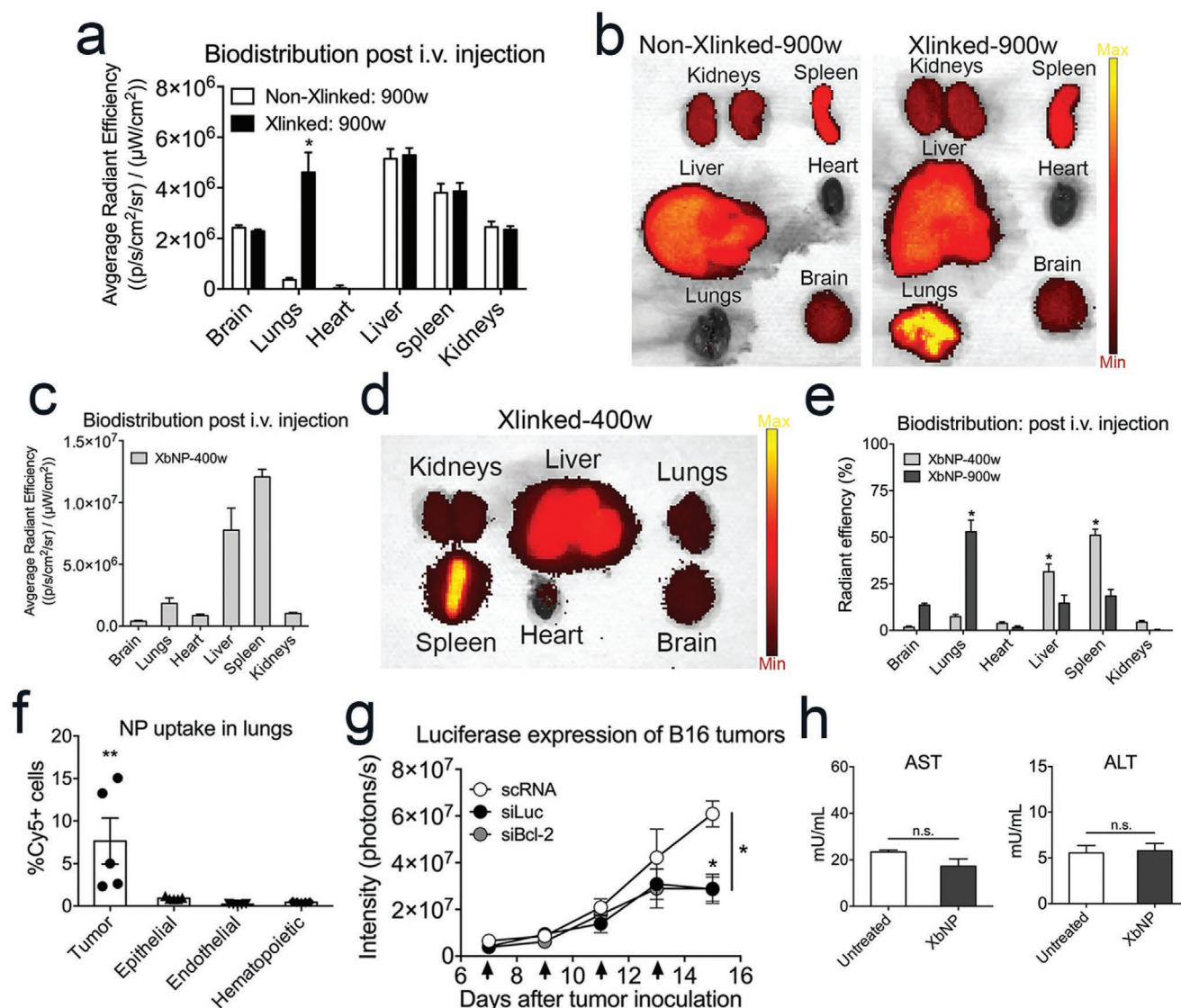
Figure 8. XbNPs enabled organ delivery beyond the liver with preferential siRNA uptake in cancer cells leading to siRNA-mediated knockdown in tumors colonized in the lungs. a) Biodistribution of nanoparticles with (Xlinked) and without (non-Xlinked) crosslinking carrying IR-labeled siRNA using formulations of 900 w/w ratios after i.v. injection and b) their representative IVIS images showing the fluorescent intensity of the IR-labeled siRNA. *$p < 0.0005$; $n = 5$; two-way ANOVA followed by Sidak's multiple comparison. c) Biodistribution of XbNPs using 400 w/w formulation ($n = 3$) and d) a representative IVIS image of the organ accumulation after i.v. injection. e) Radiant efficiency distribution based to the radiant efficiency in all of the organs for XbNPs formulations using 400 and 900 w/w. *$p < 0.01$; $n = 3$–5; two-way ANOVA followed by Sidak's multiple comparison. f) Assessment of cellular uptake in different cell types in the lungs for XbNPs carrying Cy5-labeled siRNA after i.v. injection using flow cytometry. *$p = 0.0033$; $n = 5$; one-way ANOVA followed by Tukey's post hoc test. g) Bioluminescence intensity of B16F10-Luc$^+$ cells colonized in the lungs monitored by IVIS imaging. XbNPs carrying siRNA targeting luciferase (siLuc) or Bcl-2 (siBcl-2), or scRNA as control were systemically administered 7, 9, 11, and 13 days (arrows) after tumor inoculation. *$p < 0.005$; $n = 7$; two-way ANOVA followed by Dunnett's multiple comparisons. h) Serum levels of AST and ALT, biomarkers for liver health, following four repeated injections of XbNPs or no treatment. *$p = 0.13$ (AST), *$p = 0.65$ (ALT); $n = 4$; two-tailed Student's t-test. Error bars represent SEM.

aggressive cancer cells use albumin as an essential source of energy during their outgrowth.[70,71] For instance, Cao et al. demonstrated for their nanoparticle system that pre-decoration with albumin prior to administration led to tumor-targeted delivery in metastatic breast cancer model.[48]

In a subsequent in vivo experiment, we injected B16F10-Luc$^+$ cells and allowed metastasis-like lesions to form over 7 days prior to treatment. We administered XbNPs carrying either siRNA targeting the luciferase expression, or Bcl-2 as a

therapeutic, or scRNA (control) repeatedly via i.v. injections at day 7, 9, 11, and 13 after tumor inoculation. Bcl-2 is an anti-apoptotic protein upregulated in malignant cells;[72] accordingly, silencing of Bcl-2 expression has been shown to induce apoptosis in malignant melanoma both in preclinical and clinical studies.[66,73,74] Thus, we utilized siRNA targeting luciferase (siLuc) as the bioluminescence readout gene target and Bcl-2 (siBcl-2) as therapeutic gene target. We monitored the bioluminescence from the melanoma in the lungs over time, which

demonstrated knockdown both for XbNPs carrying siLuc and siBcl-2, showing that the XbNP enabled potent systemic siRNA delivery to the melanoma cells (Figure 8g; $p < 0.005$; $n = 7$). The activity of the biomarkers aspartate aminotransferase (AST) and alanine transaminase (ALT) for liver health showed no significance difference in blood serum for animals given four repeated i.v. injections of XbNPs compared to control animals without treatment (Figure 8h). Thus, the engineered XbNPs or the presence of the photocrosslinker Irg does not cause measurable hepatotoxicity. This is likely due to the intrinsic biodegradability and bioreducibility of the polymers in the XbNP formulation, which allow quick degradation into nontoxic byproducts under aqueous or reducing conditions.[20] The low toxicity ensures safety of the nanoparticle formulation while also allowing repeated administration for effective therapeutic treatment. If in future studies in larger animals, Irg becomes a concern, it can be removed using Amicon 10 kDa MWCO filters or similar, prior to administration. Taken together, the ability of the engineered XbNPs to enable systemic delivery to metastatic melanoma tumors could open new avenues for safe and effective siRNA delivery for the unmet need of treatment of metastatic cancers. The differential organ-targeted delivery could also broaden its therapeutic potential for other diseases.

3. Conclusion

We designed XbNPs to address the main issue of colloidal stability of biodegradable cationic polymeric vehicles to broaden their use for systemic siRNA delivery. We synthesized bioreducible PBAEs to serve both for crosslinking and for payload encapsulation, with disulfide bridges facilitating environmentally triggered intracellular release. Photocrosslinking provided both improved colloidal nanoparticle stability, which improved payload encapsulation in high-serum conditions, and surface charge shielding, which reduced adsorption of anionic serum proteins. XbNPs were observed to demonstrate superior siRNA-mediated knockdown in various glioblastoma cell lines as well as in melanoma cells compared to non-crosslinked formulations in high-serum conditions. XbNPs are internalized readily by cells, which together with their enhanced stability explains their great efficacy in high serum. Another key aspect of intracellular trafficking is endosomal escape, for which the presence of both secondary and tertiary amines of XbNPs leads to efficient buffering at low pH, leading to endosomal disruption. In in vivo studies, XbNPs containing labeled siRNA targeted cancer cells and facilitated differential organ-targeted delivery through simple tuning of the polymer/siRNA ratio. In particular, formulations of XbNPs using 900 and 400 w/w formulations accumulated selectively in either the lungs or spleen, respectively, following systemic administration. XbNPs further demonstrated knockdown both when carrying siRNA targeting a reporter gene (luciferase) and the anti-apoptotic gene Bcl-2 after i.v. injections in a metastatic melanoma model, in which tumors colonized the lungs. Taken together, the improved colloidal stability, surface-charge shielding, high transfection efficacy in high-serum conditions, efficient endosomal escape, environmentally triggered nanoparticle degradation and RNA release, and overall targeted and safe in vivo delivery capacity

make XbNPs promising as a robust nanoparticle platform for systemic delivery of RNA therapeutics. The photocrosslinking strategy can also be applied generally to other cationic nanocarriers for nucleic acid delivery that rely on self-assembly to form nanoparticles for improved stability under physiological conditions.

4. Experimental Section

Materials: The chemicals used in the synthesis of the base monomer BR6 were all purchased from Sigma-Aldrich (St. Louis, MO). The other monomers used in the polymer syntheses are as follows: 4-amino-1-butanol (S4; CAS no. 13325-10-05) was purchased from Thermo Fisher Scientific (Carlsbad, CA), 2-(3-aminopropylamino)ethanol (E6; CAS no. 4461-39-6) was purchased from Sigma-Aldrich, and 1-(3-aminopropyl)-4-methylpiperazine (E7; CAS no. 4572-031) was purchased from Alfa Aesar (Ward Hill, MA). The siRNA targeting eGFP with 5′-CAAGCUGACCCUGAAGUUCTT (sense) and 3′-AACUUCAGGG-UCAGCUUGCC (antisense) (Ambion Silencer eGFP) and negative control siRNA used as the scrambled RNA (scRNA) with 5′-AGUACUGCUUACGAUACGGTT (sense) and 3′-CC-GUAUCGUAAGCAGUACUTT (anti-sense) (Ambion Silencer negative control #1) were purchased from Thermo Fisher Scientific. The siRNA targeting firefly luciferase with 5′-AGAAGGAGAUCGUGGACUAUU (sense) and 3′-UAGUCCACGAUCUCCUUCUUU (antisense) was purchased from Dharmacon (Lafayette, CO). The siRNA targeting Bcl-2 with 5′-GCAUGCGACCUCUGUUUGATT (sense) and 3′-UCAAACAGAGGUCGCAUGCTT (anti-sense) was purchased from Genepharma (Shanghai, China). Cy5-labeled siRNA (SIC005) was purchased from Sigma-Aldrich. Plasmid pCAG-GFPd2 was a gift from Connie Cepko (Addgene plasmid # 14760; http://n2t.net/addgene:14760; RRID:Addgene_14760).[75] PiggyBac transposase expression plasmid (PB200A-1) was purchased from System Biosciences (Palo Alto, CA).

Polymer Synthesis and Photocrosslinking: The bioreducible monomer 2,2′-disulfanediylbis(ethane-2,1-diyl) diacrylate (BR6) was synthesized using a method similar to that reported by Kozielski et al.[10] In brief, 2-hydroxyethyl disulfide (10 mmol) was acrylated in dichloromethane (DCM) with acryloyl chloride as the acrylation reagent (300 mmol) and in the presence of triethylamine (TEA; 300 mmol). Following overnight reaction at room temperature, the TEA HCl precipitate was removed by filtration. The product was washed with water and dried with sodium sulfate, and the solvent was removed by rotary evaporation. For the synthesis of bioreducible PBAE, the diacrylate backbone monomer BR6 and the side chain monomer 4-amino-1-butanol (S4) were dissolved in anhydrous tetrahydrofuran (THF) at a molar ratio of 1.05:1 and a total monomer concentration of 500 mg mL^{-1}. The Michael addition reaction was allowed to proceed for 24 h at 60 °C with stirring. For crosslinker preparation, the resulting acrylate-terminated base polymer R6-4-Ac was precipitated in anhydrous diethyl ether, washed twice with ether, dried under vacuum for 48 h, and dissolved in anhydrous DMSO at 100 mg mL^{-1} at –20 °C with desiccant. For preparation of amine-terminated PBAEs, the acrylate-terminated-based polymer was end-capped with either 2-(3-aminopropylamino)ethanol (E6) or 1-(3-aminopropyl)-4-methylpiperazine (E7). The end-capping molecules were dissolved in THF and added to the base polymer (0.5 M final concentration of end-cap and 167 mg mL^{-1} of base polymer) and reacted for 1 h at room temperature to form polymers R6-4-6 and R6-4-7. As above, the end-capped polymers were purified by diethyl ether precipitation and two ether washes. The remaining ether was removed by vacuum for 48 h, and the polymers were dissolved in anhydrous DMSO at 100 mg mL^{-1} and stored as aliquots at –20 °C with desiccant.

To form the nanoparticles, the polymer and siRNA were diluted separately in 25×10^{-3} M of sodium acetate buffer (NaAc; pH = 5.0) at desired concentrations. In the polymer solution, the acrylate-terminated polymer (R64-Ac) as crosslinker and end-capped polymer (R646 or R647) were mixed together and mixed with the siRNA solution. Irgacure

2959 (Irg), the radical photoinitiator, was dissolved in NaAc to a final concentration of 1.0 mg mL⁻¹. The Irg solution was mixed with the nanoparticles at a 1:1 volume ratio, and the mixture was exposed to UV light (UV lamp F15T8/BL: 15 W and wavelength of 350 nm; EIKO; Shawnee, Canada) for specified times to obtain photocrosslinked nanoparticles. Irg stock solutions were stored as 100 mg mL⁻¹ aliquots in DMSO at −20 °C until use.

Characterization of Polymers and Crosslinking: GPC and ¹H NMR: ¹H NMR was used to characterize the polymer structures and the degree of crosslinking. The polymers were dissolved in deuterated DMSO (DMSO-d_6) and nanoparticles were first lyophilized and then dissolved in DMSO-d_6 for characterization using a Bruker 500 MHz NMR and analyzed using TopSpin 3.6 software. To determine the degree of crosslinking, the acrylate peaks, which are used to form crosslinks upon exposure to UV in the presence of the photoinitiator Irg, were integrated and normalized to protons peaks in the PBAE backbone.

GPC was used to characterize the molecular weight of polymers relative to linear polystyrene standards using a refractive index detector (Waters, Milford, MA). To measure the molecular weight after crosslinking, nanoparticles were formed as described above, and then lyophilized to remove aqueous buffer. Prior to characterization, samples were dissolved in butylated hydroxytoluene-stabilized THF, filtered through a 0.2 µm polytetrafluoroethylene filter.

Nanoparticle Characterization of Physical Properties and Colloidal Stability: DLS using a Zetasizer Pro (Malvern Panalytical) was used to characterize the hydrodynamic diameter of the nanoparticle formulations. The measurements were carried out both in 1 × PBS and in 1 × PBS with low (10%) or high (50%) serum content. Measurements were carried out in PBS to characterize the influence of polymer concentration and siRNA dose on nanoparticle size and in the presence of serum to examine whether crosslinking affected particle size under physiological conditions. To assess the colloidal stability of the particle formulations when incubated in low and high serum conditions, DLS measurements were made for up to 4 h.

Zeta potential measurements were made with the same DLS instrument via electrophoretic mobility to analyze the surface charge of the nanoparticle formulations and to characterize the impact of photocrosslinking, UV exposure time, polymer concentration, and siRNA dose.

NTA and TEM were used to further analyze particle size. For the NTA experiments, nanoparticles were diluted in PBS at a 1:150 v/v ratio and then analyzed with a NanoSight NS300 (Malvern, Westborough, MA, USA) to obtain 20–100 particles per frame using the NanoSight NTA 3.2 software. For TEM, nanoparticles were prepared, and 20 µL aliquots were added to carbon-coated copper TEM grids (Electron Microscopy Sciences, Hatfield, PA, USA), then grids were washed three times for 10 s each with MilliQ water, and thereafter dried at room temperature for 10 min before they were imaged.

Lastly, a gel electrophoresis assay was performed to investigate the stability and bioreducible nature of the crosslinked particles. The crosslinked and non-crosslinked nanoparticles using 1200, 900, 300, and 200 were compared after incubation in either 50% serum for 0, 2, and 4 h or a reducing environment (10 × 10⁻³ M of GSH) for 0.25, 0.5, and 1 h. Serum alone and siRNA alone were used as controls. Samples and controls containing 167 × 10⁻⁹ M siRNA except in the serum-only control were loaded in an 1% agarose (UltraPure Agarose, Invitrogen, Carlsbad, CA) gel with 0.001 mg mL⁻¹ ethidium bromide, and the gel was run for 20 min at 100 V and imaged with UV light exposure.

Protein Adsorption: BCA and SDS–PAGE: For protein adsorption evaluation, nanoparticles were incubated with 100% serum or with PBS as a control in 1.5 mL tubes (LoBind, Eppendorf) for 1 h at 37 °C. The mixture was centrifuged at 18 000 g for 1 h at 4 °C, and the pellet was washed and then resuspended in PBS. The protein concentration was then measured using the BCA assay following the manufacturer's instructions. For analysis of individual proteins, SDS–PAGE analysis was carried out using 4–15% Mini-PROTEAN TGX Precast Protein Gels (Bio-Rad) with 1× Tris/Glycine/SDS (Bio-Rad) as the running buffer. Gel electrophoresis was run at 150 V for 45 min in a Mini-PROTEAN Tetra cell (Bio-Rad).

Cell Culture and Cell Line Preparation: GBM319 patient-derived glioblastoma cells, GL261 murine glioma cells, and B16-F10 murine melanoma cells were cultured in Dulbecco's modified Eagle's medium (DMEM; Thermo Fisher Scientific) supplemented with 10% fetal bovine serum (FBS) and 1% penicillin/streptomycin. GBM1A patient-derived glioblastoma cells were cultured as neurospheres in DMEM-F12 medium (Life Technologies) with 2% v/v B-27 serum-free supplement (Invitrogen), 1% v/v antibiotic–antimycotic, 20 ng mL⁻¹ epidermal growth factor (PeproTech, Rocky Hill, NJ, USA), and 10 ng mL⁻¹ basic fibroblast growth factor (PeproTech). For generation of reporter cell lines for optical readout for siRNA transfection experiments, a PiggyBac transposon/transposase system was used to generate cell lines constitutively expressing a destabilized form of GFP (GFPd2)[75] as described previously.[76] The PiggyBac transposon plasmid PB-CAG-GFPd2 was constructed in a laboratory and is available on Addgene (Addgene plasmid #115665; http://n2t.net/addgene:115665; RRID:Addgene_115665).[76] The PiggyBac transposon plasmid used to induce cells to express a firefly luciferase-tdTomato fusion protein (PB-fLuc = tdT, Addgene plasmid #120870; http://n2t.net/addgene:120870; RRID:Addgene_120870) was prepared from PB-GFPd2 and pcDNA3.1(+)/Luc2 = tdT using restriction enzyme cloning. pcDNA3.1(+)/Luc2 = tdT was a gift from Christopher Contag (Addgene plasmid #32904; http://n2t.net/addgene:32904; RRID:Addgene_32904).[77] PiggyBac transposase expression plasmid (PB200A-1) was purchased from System Biosciences (Palo Alto, CA). Cell lines were stably induced to express PiggyBac transposon expression cassettes as previously described and sorted to stably expressing population of cells using a Sony SH800 cytometer as previously described.[76]

siRNA Delivery In Vitro: Transfection and Viability: Cells were seeded into 96-well tissue culture plates at a density of either 5000 (B16F10), 15 000 (GBM319 and GL261), or 20 000 (GBM1A) cells per well in 100 µL complete medium and allowed to adhere overnight. GBM1A neurospheres were first dissociated into single cells and plated into wells coated with 5 µg mL⁻¹ laminin (Sigma) for 3 h at 37 °C, and cells were allowed to adhere for 48 h. Nanoparticles were formed in 25 × 10⁻³ M NaAc. For the crosslinked formulations, photoinitiator was added and UV exposure applied as described above. Each nanoparticle condition was formulated with either siRNA targeting GFP or a scrambled control siRNA (scRNA). Prior to the addition of nanoparticles, the cell culture medium was replaced with 100 µL of complete media with specified serum content (10–100%). Nanoparticles were added to each well at a 1:5 ratio of nanoparticles to medium, with a final RNA concentration of 20 × 10⁻⁹–120 × 10⁻⁹ M per well, and allowed to incubate with cells at 37 °C for 2 h, after which the mixture of particles and media was replaced with fresh complete medium. Flow cytometry was performed using a BD Accuri C6 flow cytometer (BD Biosciences) with HyperCyt autosampler to assess knockdown of GFP expression after 2 (B16F10), 4 (GL261), 5 (GBM1A), or 7 (GBM319) days. Knockdown efficacy was quantified by normalizing the geometric mean fluorescence of cells treated with siRNA to that of cells transfected with corresponding formulation containing scRNA in FlowJo ($n = 4$).

The MTS CellTiter 96 Aqueous One (Promega, Madison, WI) cell proliferation assay was performed 24 h post-transfection according to the manufacturer's instructions as a measure of cell viability. The metabolic activity of treated cells was normalized to that of untreated cells ($n = 4$).

Cellular Uptake and Endosomal Escape: Flow Cytometry, Confocal Microscopy, and Gal8 Assay: In the experiments for cellular uptake, formulations were prepared with 20% Cy5-labeled siRNA and 80% unlabeled siRNA. The nanoparticles were added to cells in media with specified serum content (50% or 100%) and allowed to incubate for 2 h, after which cells were washed with PBS and detached via trypsinization. Cells were further washed with heparin (50 µg mL⁻¹ in PBS) to remove surface-bound nanoparticles and were thereafter resuspended in FACS buffer (2% FBS in PBS) for flow cytometry analysis to quantify nanoparticle uptake.

Confocal microscopy was used to visualize nanoparticle uptake and endosomal escape. GBM319 cells were plated on Nunc Lab-Tek

8-chambered borosilicate cover-glass well plates (155411; Thermo Fisher Scientific) at 30 000 cells per well 1 day prior to transfection in 250 µL media with specified serum content (50% or 100%). The nanoparticles were prepared as described above with 20% Cy5-labeled siRNA and 80% unlabeled siRNA, and 50 µL was administered to each well and incubated with cells for 2 h. After particles and media were replaced with fresh complete media, and prior to imaging, cells were stained for 30 min with Hoechst 33342 (Thermo Fisher Scientific) nuclear stain at a 1:5000 dilution and Cell Navigator Lysosome Staining dye (AAT Bioquest, Sunnyvale, CA) at a 1:2000 dilution. Cells were washed twice and incubated in phenol-red free media, and live-cell imaging was performed at 37 °C in 5% CO_2. Images were acquired using a Zeiss LSM 780 microscope with Zen Blue software and a 63× oil immersion lens. Specific laser channels used were 405 nm diode, 488 nm argon, 561 nm solid-state, and 639 nm diode lasers. Laser intensity and detector gain settings were maintained across all image acquisitions.

The Gal8-GFP recruitment assay was performed to assess endosomal disruption/endosomal escape of nanoparticles based on a method recently reported by Kilchrist et al.[63] Briefly, B16F10 cells were engineered to constitutively express a Gal8-GFP fusion protein using the PiggyBac transposon plasmid PB-GFP-Gal8 constructed in a laboratory (Addgene plasmid #127191; http://n2t.net/addgene:127191; RRID:Addgene_127191).[78]

Nanoparticles encapsulating 20% Cy5-labeled siRNA and 80% unlabeled siRNA were incubated with cells for 2 h in media with 50% serum, after which media were replaced with fresh complete media and stained with Hoechst 33342 nuclear stain (1:5000 dilution). Gal8-GFP recruitment was analyzed using a Cellomics ArrayScan VTI with live-cell imaging module; cell count was generated using an algorithm to extrapolate the area surrounding Hoechst-stained cell nuclei, endosomal disruption was reported as the average number of punctate Gal8-GFP spots per cell, and cellular uptake reported as the average number of Cy5 spots per cell.

Animals: For the in vivo studies, 6–8 week old female C57BL/6J mice (Jackson Laboratory, Bar Harbor, ME, USA) were housed in standard facilities and were supplied with ad libitum access to food and water. All animal studies were performed in strict accordance with the NIH guidelines for the care and use of laboratory animals (NIH publication no. 85-23 Rev. 1985). The laboratory, investigators, and procedures were approved with animal protocol MO18M388 by the Animal Care and Use Committee (ACUC) of the Johns Hopkins University.

In Vivo Lung Metastasis Model, Nanoparticle Biodistribution, and Cellular Uptake: To establish metastasis-like lesions in the lungs, 100 000 B16F10 cells suspended in 100 µL of PBS were injected i.v. into mice by the lateral tail vein. To allow an optical readout of the tumor formation, B16F10-Luc=tdTomato cells were used, and tumor growth was monitored via IVIS imaging. In the biodistribution study, 7 days after tumor inoculation, nanoparticles encapsulating siRNA labeled with IR fluorescent dye (IRDye800CW; Integrated DNA Technologies, Coralville, IA, USA) were injected i.v. ($n = 3$–5). A control group ($n = 3$) was not injected with nanoparticles to account for the contribution of autofluorescence of the organs. The animals were euthanized 18 h post-administration, and the organs were collected. IVIS (PerkinElmer, Waltham, MA, USA) imaging was used to analyze the biodistribution of the fluorescent nanoparticles, and the images were analyzed in Living Image software (PerkinElmer).

In the study of cellular uptake in the lungs, tumors were established as described above using B16F10 GFPd2$^+$ cells. After 14 days, nanoparticles encapsulating Cy5-labeled siRNA were injected i.v. ($n = 4$)

to allow analysis of cellular uptake, and untreated animals were included as controls ($n = 2$). Mice were euthanized 18 h post-administration, and lungs were collected, minced, and dissociated using the Lung Dissociation kit (Miltenyi Biotec) according to the manufacturer's instructions. Red blood cells were lysed in ACK buffer, and the remaining cells were incubated for 30 min at 4 °C with antibodies against epithelial (CD326-APC/Cy7), endothelial (CD31-BV421), and immune (CD45-BV421) cell markers (all antibodies from BioLegend, San Diego, CA, USA), see **Table 1** for details. The cells were then analyzed using a CytoFlex flow cytometer (Beckman Coulter).

Efficacy and Safety for Systemically Administered Nanoparticles: To evaluate siRNA-mediated knockdown following systemic nanoparticle administration, the bioluminescence signal from the B16F10 tumors in the lungs was monitored by IVIS. Prior to imaging, 3.75 mg D-luciferin (Cayman Chemical Company) in 150 µL volume was injected intraperitoneally (i.p.) in each mouse. Image analysis was carried out using Living Image software to quantify the total bioluminescence of the colonized tumors. The nanoparticles were loaded with either siRNA targeting firefly luciferase (siLuc), siRNA targeting Bcl-2 (siBcl-2), or negative control siRNA (scRNA), and bioluminescence was used to determine whether successful delivery was achieved.

Any potential hepatotoxicity of the systemically delivered photocrosslinked nanoparticles was examined. Animals received four repeated i.v. injections of nanoparticles and untreated animals were used as controls. Blood was collected from each animal after 8 days after initiation of treatment, and the serum was collected by centrifugation at 1500 rcf for 15 min at 4 °C. The serum in treated and untreated animals was analyzed for AST activity and ALT (Sigma-Aldrich), key biomarkers for liver health. The AST and ALT activity assays were performed according to manufacturer's instructions.

Statistical Analyses: All results are presented as mean ± standard error of the mean (SEM). All statistical analyses were performed using Prism software (GraphPad Prism, San Diego, CA, USA), and $p < 0.05$ was considered statistically significant. For the analysis of the physical nanoparticle properties, one-way ANOVA followed by Tukey's post hoc test was used to compare nanoparticle size and surface charge of the different formulations. For the analysis of the total protein adsorption, two-way ANOVA followed by Sidak's multiple comparison was used. For the analyses of in vitro transfection and viability, one-way ANOVA followed by Tukey's post hoc test was used to compare the influence of UV exposure time, PBAE concentration, siRNA dose, and Irg concentration. Additionally, when comparing the transfection, cell uptake, and encapsulation efficiency of crosslinked and non-crosslinked formulations, and in the pre-incubation experiment were two-way ANOVA followed by Sidak's multiple comparison used. For the encapsulation efficiency assessed by the RiboGreen assay, Holm–Sidak corrected multiple t-tests was used. For the analysis of nanoparticle uptake in the Gal8-GFP assay, a two-tailed Student's t-test was used. For the analysis of the in vivo biodistribution, a two-way ANOVA followed by Sidak's multiple comparison was used to compare the fluorescent intensity of harvested organs. For the analysis of nanoparticle uptake in vivo, one-way ANOVA followed by Tukey's post hoc test was used to compare uptake of different cell types in the lungs. For the analysis of siRNA-mediated knockdown in metastatic B16F10-Luc$^+$ tumors, a two-way ANOVA followed by Dunnett's multiple comparison was used to examine in vivo delivery efficacy of XbNPs. For the analyses of AST and ALT activities and tdTomato expression 15 days after tumor inoculation, two-tailed Student's t-test was used.

Table 1. Antibodies used to assess cellular uptake of nanoparticles in the lungs.

Antigen	Color	Supplier	Clone	Dilution	Catalog no.	Lot no.
CD45	Brilliant Violet 421	Biolegend	30-F11	1:100	103134	B287242
CD31/PECAM	Alexa Fluor 700	Biolegend	390	1:100	102443	B303280
CD326/EpCAM	APC/Cy7	Biolegend	G8.8	1:80	118218	B266989

Supporting Information

Supporting Information is available from the Wiley Online Library or from the author.

Acknowledgements

Conflict of Interest

The authors declare no conflict of interest.

Data Availability Statement

The data that supports the findings of this study are available in the article and the supplementary material of this article. Any additional information regarding the findings of this study are available from the corresponding author upon reasonable request.

Keywords

[1] H. Yin, R. L. Kanasty, A. A. Eltoukhy, A. J. Vegas, J. R. Dorkin, D. G. Anderson, *Nat. Rev. Genet.* **2014**, *15*, 541.

[2] K. A. Whitehead, R. Langer, D. G. Anderson, *Nat. Rev. Drug Discovery* **2009**, *8*, 129.

[3] N. Bessis, F. J. GarciaCozar, M. C. Boissier, *Gene Ther.* **2004**, *11*, S10.

[4] C. E. Thomas, A. Ehrhardt, M. A. Kay, *Nat. Rev. Genet.* **2003**, *4*, 346.

[5] D. W. Pack, A. S. Hoffman, S. Pun, P. S. Stayton, *Nat. Rev. Drug Discovery* **2005**, *4*, 581.

[6] M. A. Mintzer, E. E. Simanek, *Chem. Rev.* **2009**, *109*, 259.

[7] D. Adams, A. Gonzalez-Duarte, W. D. O'Riordan, C. C. Yang, M. Ueda, A. V Kristen, I. Tournev, H. H. Schmidt, T. Coelho, J. L. Berk, K. P. Lin, G. Vita, S. Attarian, V. Plante-Bordeneuve, M. M. Mezei, J. M. Campistol, J. Buades, T. H. Brannagan, B. J. Kim, J. Oh, Y. Parman, Y. Sekijima, P. N. Hawkins, S. D. Solomon, M. Polydefkis, P. J. Dyck, P. J. Gandhi, S. Goyal, J. Chen, A. L. Strahs, S. V Nochur, M. T. Sweetser, P. P. Garg, A. K. Vaishnaw, J. A. Gollob, O. B. Suhr, *N. Engl. J. Med.* **2018**, *379*, 11.

[8] A. Akinc, M. A. Maier, M. Manoharan, K. Fitzgerald, M. Jayaraman, S. Barros, S. Ansell, X. Y. Du, M. J. Hope, T. D. Madden, B. L. Mui, S. C. Semple, Y. K. Tam, M. Ciufolini, D. Witzigmann, J. A. Kulkarni, R. van der Meel, P. R. Cullis, *Nat. Nanotechnol.* **2019**, *14*, 1084.

[9] M. Longmire, P. L. Choyke, H. Kobayashi, *Nanomedicine* **2008**, *3*, 703.

[10] K. L. Kozielski, S. Y. Tzeng, J. J. Green, *Chem. Commun.* **2013**, *49*, 5319.

[11] K. L. Kozielski, S. Y. Tzeng, B. A. Hurtado De Mendoza, J. J. Green, *ACS Nano* **2014**, *8*, 3232.

[12] J. Karlsson, Y. Rui, K. L. Kozielski, A. L. Placone, O. Choi, S. Y. Tzeng, J. Kim, J. J. Keyes, M. I. Bogorad, K. Gabrielson, H. Guerrero-Cazares, A. Quinõnes-Hinojosa, P. C. Searson, J. J. Green, *Nanoscale* **2019**, *11*, 20045.

[13] J. Karlsson, K. R. Rhodes, J. J. Green, S. Y. Tzeng, *Expert Opin. Drug Delivery* **2020**, *17*, 1395.

[14] D. Routkevitch, D. Sudhakar, M. Conge, M. Varanasi, S. Y. Tzeng, D. R. Wilson, J. J. Green, *ACS Biomater. Sci. Eng.* **2020**, *6*, 3411.

[15] D. R. Wilson, Y. Rui, K. Siddiq, D. Routkevitch, J. J. Green, *Mol. Pharmaceutics* **2019**, *16*, 655.

[16] M. Morille, C. Passirani, A. Vonarbourg, A. Clavreul, J. P. Benoit, *Biomaterials* **2008**, *29*, 3477.

[17] F. Alexis, E. Pridgen, L. K. Molnar, O. C. Farokhzad, *Mol. Pharmaceutics* **2008**, *5*, 505.

[18] A. Sizovs, L. Xue, Z. P. Tolstyka, N. P. Ingle, Y. Wu, M. Cortez, T. M. Reineke, *J. Am. Chem. Soc.* **2013**, *135*, 15417.

[19] L. Novo, E. V. B. van Gaal, E. Mastrobattista, C. F. van Nostrum, W. E. Hennink, *J. Controlled Release* **2013**, *169*, 246.

[20] J. Karlsson, H. J. Vaughan, J. J. Green, *Annu. Rev. Chem. Biomol. Eng.* **2018**, *9*, 105.

[21] H. Hatakeyama, H. Akita, E. Ito, Y. Hayashi, M. Oishi, Y. Nagasaki, R. Danev, K. Nagayama, N. Kaji, H. Kikuchi, Y. Baba, H. Harashima, *Biomaterials* **2011**, *32*, 4306.

[22] R. K. O'reilly, C. J. Hawker, K. L. Wooley, *Chem. Soc. Rev.* **2006**, *35*, 1068.

[23] N. A. Peppas, J. Z. Hilt, A. Khademhosseini, R. Langer, *Adv. Mater.* **2006**, *18*, 1345.

[24] W. E. Hennink, C. F. van Nostrum, *Adv. Drug Delivery Rev.* **2012**, *64*, 223.

[25] S. Y. Tzeng, E. B. Lavik, *Soft Matter* **2010**, *6*, 2208.

[26] O. Z. Fisher, N. A. Peppas, *Macromolecules* **2009**, *42*, 3391.

[27] O. Z. Fisher, T. Kim, S. R. Dietz, N. A. Peppas, *Pharm. Res.* **2009**, *26*, 51.

[28] D. C. Forbes, N. A. Peppas, *ACS Nano* **2014**, *8*, 2908.

[29] K. M. Luly, J. Choi, Y. Rui, J. J. Green, E. M. Jackson, *Nanomedicine* **2020**, *15*, 1805.

[30] G. M. Whitesides, J. P. Mathias, C. T. Seto, *Science* **1991**, *254*, 1312.

[31] S. Zhang, *Nat. Biotechnol.* **2003**, *21*, 1171.

[32] D. Anderson, D. Lynn, R. Langer, *Angew. Chem.* **2003**, *115*, 3261.

[33] J. J. Green, R. Langer, D. G. Anderson, *Acc. Chem. Res.* **2008**, *41*, 749.

[34] J. Sunshine, J. J. Green, K. P. Mahon, F. Yang, A. A. Eltoukhy, D. N. Nguyen, R. Langer, D. G. Anderson, *Adv. Mater.* **2009**, *21*, 4947.

[35] A. Mangraviti, S. Y. Tzeng, K. L. Kozielski, Y. Wang, Y. Jin, D. Gullotti, M. Pedone, N. Buaron, A. Liu, D. R. Wilson, S. K. Hansen, F. J. Rodriguez, G. D. Gao, F. Dimeco, H. Brem, A. Olivi, B. Tyler, J. J. Green, *ACS Nano* **2015**, *9*, 1236.

[36] H. Lopez-Bertoni, K. L. Kozielski, Y. Rui, B. Lal, H. Vaughan, D. R. Wilson, N. Mihelson, C. G. Eberhart, J. Laterra, J. J. Green, *Nano Lett.* **2018**, *18*, 4086.

[37] Y. Wang, M. Ye, R. Xie, S. Gong, *Bioconjugate Chem.* **2019**, *30*, 325.

[38] M. Goldberg, R. Langer, X. Jia, *J. Biomater. Sci., Polym. Ed.* **2007**, *18*, 241.

[39] T. L. Moore, L. Rodriguez-Lorenzo, V. Hirsch, S. Balog, D. Urban, C. Jud, B. Rothen-Rutishauser, M. Lattuada, A. Petri-Fink, *Chem. Soc. Rev.* **2015**, *44*, 6287.

[40] E. Blanco, H. Shen, M. Ferrari, *Nat. Biotechnol.* **2015**, *33*, 941.

[41] J. S. Suk, Q. G. Xu, N. Kim, J. Hanes, L. M. Ensign, *Adv. Drug Delivery Rev.* **2016**, *99*, 28.

[42] S. D. Li, L. Huang, *J. Controlled Release* **2010**, *145*, 178.

[43] T. Cedervall, I. Lynch, S. Lindman, T. Berggård, E. Thulin, H. Nilsson, K. A. Dawson, S. Linse, *Proc. Natl. Acad. Sci. USA* **2007**, *104*, 2050.

[44] D. Docter, D. Westmeier, M. Markiewicz, S. Stolte, S. K. Knauer, R. H. Stauber, *Chem. Soc. Rev.* **2015**, *44*, 6094.

[45] P. C. Ke, S. Lin, W. J. Parak, T. P. Davis, F. Caruso, *ACS Nano* **2017**, *11*, 11773.

[46] Y. Zhang, J. L. Y. Wu, J. Lazarovits, W. C. W. Chan, *J. Am. Chem. Soc.* **2020**, *142*, 8827.

[47] H. Hyun, J. Park, K. Willis, J. E. Park, L. T. Lyle, W. Lee, Y. Yeo, *Biomaterials* **2018**, *180*, 206.

[48] H. Cao, L. Zou, B. He, L. Zeng, Y. Huang, H. Yu, P. Zhang, Q. Yin, Z. Zhang, Y. Li, *Adv. Funct. Mater.* **2017**, *27*, 1605679.

[49] D. S. Manickam, J. Li, D. A. Putt, Q. H. Zhou, C. Wu, L. H. Lash, D. Oupický, *J. Controlled Release* **2010**, *141*, 77.

[50] F. Meng, W. E. Hennink, Z. Zhong, *Biomaterials* **2009**, *30*, 2180.

[51] S. Mura, J. Nicolas, P. Couvreur, *Nat. Mater.* **2013**, *12*, 991.

[52] Y. Kakizawa, A. Harada, K. Kataoka, *J. Am. Chem. Soc.* **1999**, *121*, 11247.

[53] S. Son, R. Namgung, J. Kim, K. Singha, W. J. Kim, *Acc. Chem. Res.* **2012**, *45*, 1100.

[54] X. Liu, J. Xiang, D. Zhu, L. Jiang, Z. Zhou, J. Tang, X. Liu, Y. Huang, Y. Shen, *Adv. Mater.* **2016**, *28*, 1743.

[55] A. Sukhanova, S. Bozrova, P. Sokolov, M. Berestovoy, A. Karaulov, I. Nabiev, *Nanoscale Res. Lett.* **2018**, *13*, 44.

[56] C. G. Williams, A. N. Malik, T. K. Kim, P. N. Manson, J. H. Elisseeff, *Biomaterials* **2005**, *26*, 1211.

[57] A. Soeda, A. Hara, T. Kunisada, S. I. Yoshimura, T. Iwama, D. M. Park, *Sci. Rep.* **2015**, *5*, 7979.

[58] J. Tilghman, H. Wu, Y. Sang, X. Shi, H. Guerrero-Cazares, A. Quinones-Hinojosa, C. G. Eberhart, J. Laterra, M. Ying, *Cancer Res.* **2014**, *74*, 3168.

[59] S. Bao, Q. Wu, R. E. McLendon, Y. Hao, Q. Shi, A. B. Hjelmeland, M. W. Dewhirst, D. D. Bigner, J. N. Rich, *Nature* **2006**, *444*, 756.

[60] D. M. Park, J. N. Rich, *Mol. Cells* **2009**, *28*, 7.

[61] S. A. Smith, L. I. Selby, A. P. R. Johnston, G. K. Such, *Bioconjugate Chem.* **2019**, *30*, 263.

[62] L. M. P. Vermeulen, S. C. De Smedt, K. Remaut, K. Braeckmans, *Eur. J. Pharm. Biopharm.* **2018**, *129*, 184.

[63] K. V Kilchrist, S. C. Dimobi, M. A. Jackson, B. C. Evans, T. A. Werfel, E. A. Dailing, S. K. Bedingfield, I. B. Kelly, C. L. Duvall, *ACS Nano* **2019**, *13*, 1136.

[64] T. Lin, P. Zhao, Y. Jiang, Y. Tang, H. Jin, Z. Pan, H. He, V. C. Yang, Y. Huang, *ACS Nano* **2016**, *10*, 9999.

[65] Q. Cheng, T. Wei, L. Farbiak, L. T. Johnson, S. A. Dilliard, D. J. Siegwart, *Nat. Nanotechnol.* **2020**, *15*, 313.

[66] B. Zbytek, J. A. Carlson, J. Granese, J. Ross, M. C. Mihm, A. Slominski, *Expert Rev. Dermatol.* **2008**, *3*, 569.

[67] C. G. Zamboni, K. L. Kozielski, H. J. Vaughan, M. M. Nakata, J. Kim, L. J. Higgins, M. G. Pomper, J. J. Green, *J. Controlled Release* **2017**, *263*, 18.

[68] S. Y. Tzeng, L. J. Higgins, M. G. Pomper, J. J. Green, *J. Biomed. Mater. Res., Part A* **2013**, *101A*, 1837.

[69] S. Y. Tzeng, H. Guerrero-Cázares, E. E. Martinez, J. C. Sunshine, A. Quiñones-Hinojosa Alfredo, J. J. Green, *Biomaterials* **2011**, *32*, 5402.

[70] A. M. Merlot, D. S. Kalinowski, D. R. Richardson, *Front. Physiol.* **2014**, *5*, 299.

[71] M. S. Dennis, H. Jin, D. Dugger, R. Yang, L. McFarland, A. Ogasawara, S. Williams, M. J. Cole, S. Ross, R. Schwall, *Cancer Res.* **2007**, *67*, 254.

[72] C. F. A. Warren, M. W. Wong-Brown, N. A. Bowden, *Cell Death Dis.* **2019**, *10*, 177.

[73] Z. Zhou, H. Li, K. Wang, Q. Guo, C. Li, H. Jiang, Y. Hu, D. Oupicky, M. Sun, *ACS Appl. Mater. Interfaces* **2017**, *9*, 14576.

[74] A. Y. Bedikian, M. Millward, H. Pehamberger, R. Conry, M. Gore, U. Trefzer, A. C. Pavlick, R. DeConti, E. M. Hersh, P. Hersey, J. M. Kirkwood, F. G. Haluska, *J. Clin. Oncol.* **2006**, *24*, 4738.

[75] T. Matsuda, C. L. Cepko, *Proc. Natl. Acad. Sci. USA* **2007**, *104*, 1027.

[76] Y. Rui, D. R. Wilson, K. Sanders, J. J. Green, *ACS Appl. Mater. Interfaces* **2019**, *11*, 10472.

[77] M. R. Patel, Y. F. Chang, I. Y. Chen, M. H. Bachmann, X. Yan, C. H. Contag, S. S. Gambhir, *Cancer Res.* **2010**, *70*, 10141.

[78] Y. Rui, D. R. Wilson, J. Choi, M. Varanasi, K. Sanders, J. Karlsson, M. Lim, J. J. Green, *Sci. Adv.* **2019**, *5*, eaay3255.